1521-0103/358/3/371–386$25.00
THE JOURNAL OF PHARMACOLOGY AND EXPERIMENTAL THERAPEUTICS

http://dx.doi.org/10.1124/jpet.116.235333
J Pharmacol Exp Ther 358:371–386, September 2016

Inhibition of AAK1 Kinase as a Novel Therapeutic Approach to Treat Neuropathic Pain[S]

Walter Kostich,[1] Brian D. Hamman,[1] Yu-Wen Li, Sreenivasulu Naidu, Kumaran Dandapani, Jianlin Feng, Amy Easton, Clotilde Bourin, Kevin Baker, Jason Allen, Katerina Savelieva, Justin V. Louis, Manoj Dokania, Saravanan Elavazhagan, Pradeep Vattikundala, Vivek Sharma, Manish Lal Das, Ganesh Shankar, Anoop Kumar, Vinay K. Holenarsipur, Michael Gulianello, Ted Molski, Jeffrey M. Brown, Martin Lewis, Yanling Huang, Yifeng Lu, Rick Pieschl, Kevin O'Malley, Jonathan Lippy, Amr Nouraldeen, Thomas H. Lanthorn, Guilan Ye, Alan Wilson, Anand Balakrishnan, Rex Denton, James E. Grace, Kimberley A. Lentz, Kenneth S. Santone, Yingzhi Bi, Alan Main, Jon Swaffield, Ken Carson, Sandhya Mandlekar, Reeba K. Vikramadithyan, Susheel J. Nara, Carolyn Dzierba, Joanne Bronson, John E. Macor, Robert Zaczek, Ryan Westphal, Laszlo Kiss, Linda Bristow, Charles M. Conway, Brian Zambrowicz, and Charles F. Albright

Research and Development, Neuroscience Biology (W.K., Y.-W.L., J.F., A.E., C.B., M.G., T.M., J.M.B., M.L., Y.H., Y.L., R.P., R.Z., R.W., L.K., L.B., C.M.C., C.F.A.), Neuroscience Chemistry (C.D., J.B., J.E.M.), Preclinical Candidate Optimization (A.B., J.E.G., K.A.L., K.S.S.), and Discovery Toxicology (R.D.), Bristol-Myers Squibb, Wallingford, Connecticut; Research and Development, Leads Discovery and Optimization, Bristol-Myers Squibb, Pennington, New Jersey (K.O., J.L.); BMS Biocon Research Center, Bangalore, India (K.D., J.V.L., S.N., M.D., S.E., P.V., V.S., M.L.D, G.S., A.K., V.K.H., S.M., R.K.V., S.J.N.); Lexicon Pharmaceuticals, The Woodlands, Texas (B.D.H., K.B., J.A., K.S., A.N., A.W., J.S., B.Z., T.H.L., G.Y.); and Lexicon Pharmaceuticals, Basking Ridge, New Jersey (Y.B., A.M., K.C.)

Received May 19, 2016; accepted July 6, 2016

ABSTRACT

To identify novel targets for neuropathic pain, 3097 mouse knockout lines were tested in acute and persistent pain behavior assays. One of the lines from this screen, which contained a null allele of the adapter protein-2 associated kinase 1 (AAK1) gene, had a normal response in acute pain assays (hot plate, phase I formalin), but a markedly reduced response to persistent pain in phase II formalin. AAK1 knockout mice also failed to develop tactile allodynia following the Chung procedure of spinal nerve ligation (SNL). Based on these findings, potent, small-molecule inhibitors of AAK1 were identified. Studies in mice showed that one such inhibitor, LP-935509, caused a reduced pain response in phase II formalin and reversed fully established pain behavior following the SNL procedure. Further studies showed that the inhibitor also reduced evoked pain responses in the rat chronic constriction injury (CCI) model and the rat streptozotocin model of diabetic peripheral neuropathy. Using a nonbrain-penetrant AAK1 inhibitor and local administration of an AAK1 inhibitor, the relevant pool of AAK1 for antineuropathic action was found to be in the spinal cord. Consistent with these results, AAK1 inhibitors dose-dependently reduced the increased spontaneous neural activity in the spinal cord caused by CCI and blocked the development of windup induced by repeated electrical stimulation of the paw. The mechanism of AAK1 antinociception was further investigated with inhibitors of α2 adrenergic and opioid receptors. These studies showed that α2 adrenergic receptor inhibitors, but not opioid receptor inhibitors, not only prevented AAK1 inhibitor antineuropathic action in behavioral assays, but also blocked the AAK1 inhibitor–induced reduction in spinal neural activity in the rat CCI model. Hence, AAK1 inhibitors are a novel therapeutic approach to neuropathic pain with activity in animal models that is mechanistically linked (behaviorally and electrophysiologically) to α2 adrenergic signaling, a pathway known to be antinociceptive in humans.

Introduction

Neuropathic pain is caused by a lesion or disease of the somatosensory nervous system (reviewed in Costigan et al., 2009), such as herpes infection and diabetes, which can lead to postherpetic neuralgia and diabetic peripheral neuropathy, respectively. As a consequence of these conditions, patients can experience hyperalgesia (increased pain from a normally

This work was supported by Bristol-Myers Squibb and Lexicon Pharmaceuticals.
All authors were employees of either Bristol-Myers Squibb or Lexicon Pharmaceuticals at the time when this work was done; many authors own in excess of $10,000 of company stock. Additionally, some authors are inventors on patents related to the subject matter.
[1]W.K. and B.D.H. contributed equally to this work.
dx.doi.org/10.1124/jpet.116.235333.
[S] This article has supplemental material available at jpet.aspetjournals.org.

painful stimulus), allodynia (pain due to a stimulus that does not normally evoke pain), and spontaneous pain (pain arising without an obvious triggering event).

Neuropathic pain is commonly treated with tricyclic antidepressants, serotonin-norepinephrine reuptake inhibitors (SNRI), and gabapentinoids (Costigan et al., 2009; Finnerup et al., 2010). The antinociceptive mechanism of these medications is linked to the endogenous noradrenergic system, which is a powerful inhibitor of spinal dorsal horn circuits required for neuropathic pain (reviewed in Fairbanks et al., 2009). In particular, the endogenous system originates primarily from the locus ceruleus, where descending neurons project to the dorsal horn. When stimulated, these neurons release norepinephrine, which binds to α2 adrenergic receptors. Binding of norepinephrine to α2A-adrenergic receptors on presynaptic afferent terminals reduces substance P and glutamate release from primary afferents via the cholinergic pathways. Binding of norepinephrine to α2C-adrenergic receptors on postsynaptic secondary neurons causes hyperpolarization by G protein activation of G-protein gated inward rectifier potassium (GIRK) potassium channels. Gabapentinoids activate the descending inhibitory neurons in the locus ceruleus (Hayashida et al., 2008). In addition, gabapentinoids bind and affect the subcellular trafficking of $\alpha 2\delta$-1 subunits of calcium channels, thereby preventing the pain-induced increase in calcium currents (Dolphin, 2012). SNRIs and tricyclic antidepressants cause antinociception by increasing the dorsal horn concentration of serotonin and norephinephrine by inhibiting their reuptake from the synapse (Benarroch, 2008). The α2A adrenergic and the α2C adrenergic receptors can be activated directly with an α2 adrenergic agonist, such as clonidine. Although clonidine is used intrathecally as an opioid adjuvant for postoperative pain (Engelman and Marsala, 2013), broader clonidine usage for pain reduction is limited by sedation and hypotension. Consistent with a pathway linkage between these antinociceptives, α2 adrenergic antagonists prevent antinociception by gabapentin (Hayashida et al., 2007), SNRIs (Obata et al., 2005), and α2 adrenergic agonists (Fairbanks et al., 2009).

Despite the presence of marketed therapeutics for neuropathic pain, a significant unmet need remains. Importantly, the existing therapeutic compounds do not eliminate neuropathic pain for most patients (Finnerup et al., 2010). Specifically, less than half of neuropathic pain patients achieve a 50% reduction in pain with current treatments (Snedecor et al., 2014). Furthermore, current treatments frequently have undesired side effects such as weight gain from tricylic antidepressants and sedation plus cognitive impairment from gabapentinoids.

Given the significant unmet need, we screened knockout mice to identify novel pain targets. This strategy was based on a retrospective evaluation of the knockout phenotypes for the targets of the 100 best-selling drugs that showed that these phenotypes correlated well with known drug efficacy (Zambrowicz and Sands, 2003). The general phenotypic screen (Beltran del Rio et al., 2003; Tang et al., 2010), as well as the obesity (Brommage et al., 2008), diabetes (Powell et al., 2013), and bone (Brommage et al., 2014) components of this screen, was previously described, and datasets for 472 gene knockout lines were made publicly available (Tang et al., 2010). The pain component of this screen consisted of hot-plate and formalin-paw assays, both semiautomated assays amenable to screening large numbers of animals. The formalin assay assessed the inflammatory and central sensitization components in addition to the acute pain addressed by the hot-plate assay (Mogil, 2009). Using the formalin assay, AP2-associated kinase 1 (AAK1) knockouts were identified based on their reduced response to persistent pain. Based on these AAK1 knockout results, we created selective, small-molecule inhibitors of AAK1, a kinase implicated in endocytosis (Conner and Schmid, 2002). These AAK1 inhibitors recapitulated the knockout phenotype and reversed animal behaviors consistent with the relief of neuropathic pain. In addition, AAK1 inhibitors suppressed the increase in spontaneous action potentials following chronic constriction injury (CCI) nerve injury and prevented the development of windup normally induced by repeated electrical stimulation of afferents that innervate spinal dorsal horn cells. These AAK1 inhibitors were then used to behaviorally and electrophysiologically link the mechanism of pain reversal to adrenergic signaling in the spinal cord.

Materials and Methods

Synthesis of AAK1 Inhibitors

Experimental details and procedures for the synthesis of LP-935509, LP-922761, BMT-090605, BMT-124110, LP-927443, and BMS-901715 and full characterization (1H NMR, 13C NMR, low- or high-resolution mass spectrometry, optical rotation, and melting point) of final compounds are described in Supplemental Material.

AAK1 Protein Expression and Biochemical Assays

AAK1 protein was expressed using a recombinant baculovirus and purified, and kinase activity was determined using biochemical assays described in Supplemental Material. BMP-2-inducible protein kinase (BIKE) and Cyclin G-associated kinase (GAK) kinases were expressed, and kinase activity was determined, as described in Supplemental Material.

AAK1 Cellular Assays

AAK1 was transiently expressed in HEK293F cells together with adaptor protein 2 (AP-2), an AAK1 kinase substrate. The extent of inhibition of AP-2 phosphorylation at various compound concentrations was then determined by Western blotting. Detailed methods are described in Supplemental Material.

AAK1 Knockout Behavior and In Vivo Pharmacology

All of the animals were kept in an American Association for the Accreditation of Laboratory Animal Care–accredited animal holding facility maintained at controlled temperature (23 ± 1°C) and humidity (50 ± 20%) under a 12:12 hour light:dark cycle (lights on at 07:00 hours). Food and water were provided ad libitum. All experimental procedures were reviewed and approved by the Institutional Animal Ethics Committee and conducted in accordance with procedures set by the Committee for the Purpose of Control and Supervision on Experiments on Animals. AAK1 knockout mice were generated on a C57 × 129 hybrid background strain. Exon 2 of the AAK1 gene was deleted using gene targeting by homologous recombination in 129/SvEvBrd embryonic stem cells and confirmed by Southern blot.

ABBREVIATIONS: AAK1, adapter protein-2 associated kinase 1; AP-2, adaptor protein 2; CCI, chronic constriction injury; GABA, γ-aminobutyric acid; LV, lumbar vertebrae; PK, pharmacokinetic; SNL, spinal nerve ligation; SNRI, serotonin-norepinephrine reuptake inhibitor; STZ, streptozotocin.

Chimeras were bred to C57BL/6J mice, and heterozygous mice were intercrossed. An additional null allele was produced by gene trapping (OST 23,964). Both alleles exhibited similar phenotypes (data not shown), and the work described in this paper was carried out with the gene-targeted allele. Mice used for LP-935509 in vivo pharmacology studies were of the C57BL/6J albino strain (Ye et al., 2015). The formalin-paw test was used to assess acute and tonic nociceptive responses in mice. A metal band was placed around the left hind paw of each mouse, and 20 μl 5% formalin was s.c. injected in the dorsal surface of the left hind paw. Mice were individually housed in cylindrical chambers for 45 minutes. A computer recorded flinches per minute, total flinches for phase I (acute phase = first 8 minutes), and total flinches for phase II (tonic phase between 20 and 40 minutes) through an electromagnetic field. In the primary screen, four knockout animals and four littermate controls for each line were tested to identify potential phenotypes that could then be followed up in larger cohorts. Some knockout lines were not screened due to embryonic lethality or timing of implementation of the formalin test.

LP-935509 Drug Administration

For all mouse studies, LP-935509 was formulated in 10% Cremophor and dosed orally at 10, 30, and 60 mg/kg (10 ml/kg). Gabapentin (G154Sigma from Sigma-Aldrich, St. Louis, MO) was freshly dissolved in sterile saline and administered orally at 200 mg/kg (10 ml/kg). Both drugs were given 30 minutes prior to the formalin injection or prior to von Frey testing. Mice were tested for baseline von Frey sensitivity 24 hours prior to the validation study. The mice that met the following selection criteria were included in the drug validation experiment: 1) von Frey 50% threshold for ipsilateral paw <1, and 2) 50% threshold for contralateral paw >2. Von Frey testing was performed at 0, 30, and 120 minutes after LP-935509 dosing.

For all rat studies [with the exception of the pharmacokinetic (PK) and rotarod experiments], LP-935509 was formulated in 40% polyethylene glycol, 10% ethanol, 15% Tween 80, and 35% water and delivered orally at the specified dose and a volume of 3 ml/kg. In the PK and rotarod studies, LP-935509 was prepared in 10% Cremophor EL in water. Gabapentin was formulated in 40% polyethylene glycol, 10% ethanol, 15% Tween 80, and 35% water for all rat studies, except the rotarod study, in which case it was prepared in 25% Captisol, 0.1 M citrate buffer (pH 3.0).

Administration of Other Drugs

Morphine and naloxone were dissolved in saline and each delivered s.c. at 3 mg/kg and 1 mg/kg, respectively, in a volume of 3 ml/kg. Yohimbine and tizanidine were dissolved in saline and each delivered i.p. at 1 mg/kg in a volume of 2 ml/kg. BMT-090605 and clonidine were dissolved in artificial cerebrospinal fluid with HEPES buffer in preparation for intrathecal dosing. Final dosing volume for both was 10 μl. LP-922761 was formulated in 10% Cremophor and dosed orally for the mouse spinal nerve ligation (SNL) study (10 ml/kg).

Open-Field Assay in Mice

Mice were acclimated to the experimental room illuminated at 30 lux for 30 minutes. Mice were then placed into the testing chamber containing infrared sensors along the perimeter (Montana et al., 2011). Locomotor activity, counted with each beam break, was recorded for 30 minutes using automated software (Accuscan). The sum activity detected over the 30-minute period was used for statistical analysis. The chambers were cleaned with 70% ethanol between test sessions.

Formalin Assay in Mice

Persistent pain or hyperalgesia can be induced with an injection of formalin into the dorsum of the hind paw, as previously described (Dubuisson and Dennis, 1977). To measure hyperalgesia in AAK1 knockout mice, a metal band was placed around the right hind paw of each mouse prior to testing. After a 30-minute acclimation period to an individual cylindrical test chamber, 20 μl 5% formalin in saline (Sigma-Aldrich) was s.c. injected in the dorsal surface of the right hind paw. Mice were immediately placed back into the test chamber where movement of the metal band breaks the electromagnetic field of a loop antenna located under the mouse and is automatically recorded as a flinch. The receiver output is amplified, filtered, and digitized for analysis using the Automated Nociception Analyzer (Yaksh et al., 2001) (Ozaki laboratory, University of California, San Diego, CA). Flinches were recorded for 60 minutes. The mouse displays a biphasic incidence of flinching (phase I or acute phase was defined as 0–9 minutes, and phase II or tonic phase was defined as 10–60 minutes, as indicated), and the data from each phase are summed for statistical analysis and graphical representation. For testing compounds, slight modifications were made to the protocol. In these studies, investigatory compounds were administered 30 minutes prior to formalin injection. The left hind paw was injected with fresh 5% formalin prepared by diluting formaldehyde (Formalde-fresh 20%; Fisher Scientific, Fair Lawn, NJ) with distilled water. Phase II data included the sum of flinches between 20 and 40 minutes after the formalin injection.

SNL in Mice

Methods for mouse SNL were carried out according to the procedures devised by Kim and Chung (1992) with modifications, as published previously (Kim and Chung, 1992; Ye et al., 2015). At 5–7 weeks of age, male mice were anesthetized with isoflurane (2% at the oxygen flow rate of 1 ml/min). A skin incision (1 cm) was made 1 mm to the left of the dorsal midline, using the level of iliac crests as the midpoint of the incision. The paraspinal muscles were bluntly separated medial to the iliac crest to reveal transverse processes between the caudal edge of lumbar level four (L4) and the rostral edge of L6 [or sacroiliac junction in mice that had only five lumbar vertebrae (LV)]. This approach facilitated identification of spinal nerves L4, L5, and/or L6. The position of the last two lumbar transverse processes in relation to the iliac crest was used to differentiate mice with five LV from those with six. Using these bone landmarks, the number of LV that a mouse possesses was accurately identified in the majority of cases. Ligation of the L4 and L5 spinal nerves was performed by passing a suture under L5 with one pair of fine forceps and pulling the suture out from the other side with another pair of fine forceps. After hemostasis was confirmed, the incision was closed in two layers, with 5-0 vicryl suture for the dorsolumbar fascia and wound clips for the skin. In sham-operated animals, the surgical procedure was identical to that as described above, except that spinal nerves were not ligated. Mice were given an injection of saline (1 ml) and buprenorphine (0.05–0.1 mg/kg mice) immediately following the surgery and buprenorphine again at approximately 12 and 24 hours postsurgery (for a total of three doses) to relieve surgery-induced pain. A warming pad at 36 $\pm$ 1°C and a heating lamp were used to maintain normal body temperature of the animal throughout the surgery. Mice were individually housed after the procedure and were monitored until complete recovery from anesthesia. For drug studies, mice were tested 3–4 weeks postsurgery.

Mechanical Allodynia in Mice via Manual von Frey

Mechanical allodynia was assessed by testing the hind paw withdrawal response (withdrawal, flinching, licking) to a set of von Frey filaments (numbered 2.44, 2.83, 3.22, 3.61, 4.08, and 4.31 corresponding approximately to force of 0.04, 0.07, 0.16, 0.4, 1, and 2 g; Stoelting, Wood Dale, IL) in an up-down procedure, as described by Chaplan et al. (1994). Baseline von Frey tests were carried out 24 hours prior to surgery and repeated once per week for 3–6 weeks after surgery depending on experimental design. For the von Frey tests, mice were placed in transparent polyethylene terephthalate cylinders with a wire mesh floor to allow the experimenter to apply the

von Frey filament to the mouse plantar surface. Both paws were tested. The first von Frey filament applied was 3.61. If no response was elicited, the next stronger filament was presented. If there was a response, the next weaker filament was presented. There were total of six presentations of von Frey filaments. If the animal did not respond to the strongest filament, 4.31, the test was ended. The 50% withdrawal threshold was calculated for each paw using the up-down method. Mice that exhibited 50% withdrawal threshold below 2 in any paw during baseline testing were excluded from surgery and further assessment. Von Frey test experimenters were always blind to the nature of the surgery and the treatment.

CCI in Rats

On the day of surgery, male Sprague-Dawley rats were transferred from the holding area to an aseptic surgery suite. Animals were anesthetized with 2% isoflurane and placed in the prone position, and the left hind limb was supported and immobilized with adhesive tape. Following shaving of the fur and disinfection of the surgical site with betadine, a small incision was made in the mid-posterior thigh to expose the sciatic nerve. Four ligations, made of 4-0 chromic gut, were loosely tied around the nerve 1–2 mm apart without interrupting the epineural blood supply (Bennett and Xie, 1988). A sham group of rats underwent a similar surgical procedure but without the nerve ligation. On completion of the procedure, the incision was closed with surgical thread, topical disinfectant (povidone-iodine solution i.p.) was applied locally, and Gentamicin (4 mg/kg) was administered s.c. Animals were initially housed individually and then pair-housed 3 days after surgery until behavioral testing. Separate groups of rats were evaluated for thermal hyperalgesia, cold allodynia, mechanical hyperalgesia, or mechanical allodynia 2–4 weeks postsurgery.

Streptozotocin-Induced Diabetic Peripheral Neuropathic Pain in Rats

Male Sprague-Dawley rats were fasted overnight and then treated with 50 mg/kg streptozotocin (STZ) prepared in 0.1 M citrate buffer (pH 4.5) (Courteix et al., 1993). Rats were allowed food 1 hour after STZ treatment and were monitored for the next 48 hours for any symptoms of hypoglycemia. Animals were evaluated for mechanical allodynia beginning 5–6 weeks post-STZ administration. Hyperglycemia, defined as a plasma glucose level >250 mg/dL, was confirmed in all subjects prior to testing.

Thermal Hyperalgesia in Rats

Thermal hyperalgesia was measured using the Hargreaves plantar test (Hargreaves et al., 1988). On the test day, CCI rats were acclimatized for 1 hour to the experimental room and then placed in observational boxes situated on a temperature-regulated platform maintained at 30°C for 30 minutes. The paw withdrawal latency following application of a radiant heat source of 35% intensity was measured for three trials (intertrial interval = 5–10 minutes), and the average latency was calculated at each time point for each subject. To prevent tissue damage, a cutoff time of 30-second radiant heat application was used.

Cold Allodynia in Rats

Cold allodynia was assessed using a cold- and hot-plate antinociception meter (IITC Life Science Incremental Hot Cold Plate Analgesia Meter). On the test day, rats were acclimatized for 1 hour to the experimental room and then placed into an observational box for 5 minutes. The latency to the first brisk lift/withdrawal or licking/guarding of the hind paw was recorded at 10°C. A general limb movement involving coordinated movement of all four limbs (e.g., walking) was not considered as a withdrawal response. To prevent tissue damage, a maximum cutoff time limit of 100 seconds was used (Tanimoto-Mori et al., 2008).

Mechanical Allodynia in Rats

Manual von Frey. For CCI studies, rats were acclimatized for 1 hour to the experimental room and then placed into observational boxes with wire-mesh floors for 20 minutes. Paw withdrawal threshold was recorded using a series of von Frey hairs with a force of 0.4 g, 0.8 g, 1.5 g, 2.5 g, 4 g, 8 g, 10 g, and 20 g (IITC Life Science, Woodland Hills, CA; model 2390 series) applied perpendicularly to the midplantar surface (Chaplan et al., 1994). Brisk paw withdrawal or licking immediate after pressure application was defined as a positive response, and lack of paw withdrawal within 6 seconds was defined as a negative response. Ambulation was considered an ambiguous response, and in such cases the stimulus was repeated. Both CCI/sham groups of rats were evaluated for paw withdrawal threshold 2 weeks postsurgery.

Electronic von Frey. For STZ studies, rats were first acclimatized for 1 hour to the experimental room and then placed into observational boxes with wire-mesh floors for 20 minutes. Paw withdrawal threshold was recorded using an electronic von Frey Aesthesiometer (model no. series 2390; IITC Life Science). The rigid electronic von Frey hair was applied to the midplantar surface with an ascending force for 6 seconds. The maximum force at which the animal shows a withdrawal/licking response was recorded as the paw withdrawal threshold, as shown on the digital display. Withdrawal thresholds for each hind paw were measured in two trials with an intertrial interval of 5 minutes. The mean paw withdrawal threshold (g) of all four trials was calculated for each time point (Morrow, 2004).

Mechanical Hyperalgesia in Rats

Rats were handled before commencing the study, placed in a sling suit, and allowed to acclimatize for 20 seconds. Mechanical hyperalgesia was assessed using a digital paw pressure Randall Selitto instrument (IITC Life Science). An incremental pressure was applied to the plantar surface of the paw. Increasing force was applied until a vocalization/withdrawal response was observed with a 250 g cutoff applied to prevent tissue damage. The withdrawal threshold was measured in two trials (5-minute intertrial interval), and all four readings were averaged to determine the mean nociceptive threshold (g) (Santos-Nogueira et al., 2012).

Rat Tail-Flick Assay

Rats were transferred to the experimental room to acclimate for 1 hour and then selected randomly for testing (D'Amour and Smith, 1941). A radiant heat source (Panlab, LE7106 analgesia meter) was focused on the marked area of tail approximately 5 cm from the distal end of the tail while the animals were held. When the animal flicked his tail in response to the heat, the instrument stopped radiation and the time was noted as the tail-flick latency. Three latency measurements were taken per animal separated by at least 5 minutes and were averaged to determine the final latency. A maximum cutoff time of 10 seconds was used to avoid injury. Animals were tested 30 minutes after morphine administration and 90 minutes after LP-533509 or vehicle administration. To evaluate the analgesic response, pretreatment latency was compared with post-treatment latency using paired t test. Data are expressed as the mean ± S.E.M. with $P < 0.05$ being considered statistically significant.

Rat Hot-Plate Assay

Animals were acclimatized to the hot plate for 15 minutes 1 day before the test (Woolfe and MacDonald, 1944). On the test day, individual rats were placed on a hot plate (BIOSEB) 55 ± 1°C with a cutoff time of 30 seconds. Latency to response, such as lifting or licking a hind paw, jumping, or vocalization, was recorded. Baseline latency was recorded before the treatment. Animals were then administered morphine, LP-935509, or vehicle, and the latency was recorded 30 minutes (morphine) or 90 minutes (LP-935509 and vehicle) postdosing. Three latencies were measured at a minimum of

5-minute intervals and were averaged to determine the final latency. To evaluate the analgesic response, pretreatment latency was compared with post-treatment latency using paired t test. Data are expressed as the mean ± S.E.M. with $P < 0.05$ being considered statistically significant.

Rotarod Assay

Rotarod performance was measured using a Rotamex 5 instrument in male naive Sprague-Dawley rats (230–250 g) (Dunham and Miya, 1957; Watzman et al., 1964). Rats were trained for 3 consecutive days on the accelerating rod for 5 minutes. The training session consisted of two trials per day, one each in the morning and in the afternoon, in which the rat was placed on a horizontally oriented accelerated rotating rod configured to accelerate at a speed of 2–20 rpm over 5 minutes. Each day's second training session ended with an additional training of 30 seconds at 0–14 rpm speed. On the test day, the rats were acclimated to the testing room for 1 hour, followed by dosing with vehicle or drug. At 1, 3, and 5 hours post-treatment, rats were placed on the accelerating rotarod, and time spent on the rotating beam before falling was recorded in a 5-minute test session. Animals able to remain on the rotarod for the entire test session were given a score of 300 seconds.

Intrathecal Injection

A rat was held firmly from the pelvic girdle with one hand while a 25 μl glass Hamilton syringe with 25-ga needle was positioned and inserted between L4 and L5 of the spinal process at 75–80° angle relative to taut skin plane (Hylden and Wilcox, 1980; Mestre et al., 1994). Once the injector sensed the bone, the needle was lowered to an approximately 30° angle and slipped between the vertebrae (Fairbanks, 2003). The solution was then injected very slowly in a volume of 10 μl, and the needle rotated on withdrawal. The tip of the needle was inserted in such a way as approximately 0.5 cm was within the vertebral column. Test compounds were prepared in artificial cerebrospinal fluid with HEPES buffer.

In Vivo Spinal Electrophysiology

Rats were anesthetized with isoflurane (5% induction, 2–3% maintenance) and paralyzed with pancuronium (1 mg/kg i.v.). Animals were artificially ventilated, and the arterial pressure was monitored. A laminectomy was performed at the L1–5 vertebral level to expose the spinal cord, and a carbon fiber-recording electrode (Kation Scientific, Minneapolis, MN)) was inserted into lamina V of the dorsal horn using a SCAT microdrive (FHC, Bowdoin, ME). Extracellular action potential spikes (either spontaneous or evoked) from single neurons were isolated, amplified, and filtered using ExAmp-20KB (Kation Scientific). The spike activities were acquired and analyzed using a CED 1401 interface and Spike 2 software (Cambridge Electronic Design, Cambridge, UK). In experiments in which CCI rats were used, electrophysiological recordings were carried out in the rats 2–5 weeks postsurgery. In these animals, spontaneous action potential spikes were recorded in the dorsal horn ipsilateral to the side of the sciatic ligation, and spike frequencies were determined. In the windup studies in which naive rats were used, wide-dynamic range cells in the dorsal horn were identified according to their responses to innocuous mechanical (brushing hind paw skin) and noxious (pinching of the skin) stimuli. Trains of electrical stimuli (16 pulses, 2.0-ms duration, 2 nA intensity, 5-minute interval) were applied through a pair of fine needle electrodes inserted s.c. into the receptive field of the plantar skin, and the stimulus intensity was set to activate C-fiber–mediated spike activation.

LP-935509 and yohimbine were administrated by i.v. bolus injections. For the microiontophoresis test, double-barrel microelectrodes were inserted to the dorsal horn with one (carbon electrode) to record single neuronal spike activity and another (glass barrel) to focally administer BMT-124110 by microiontophoresis (30 mM, pH 4, +10–30 nA, 3 minutes).

Results

AAK1 Knockout Mice Have an Antinociceptive Phenotype in the Formalin Assay and SNL Model. To identify novel therapeutic targets for neuropathic pain, 3097 homozygous mouse knockout lines representing the druggable genome (Brommage et al., 2014) were tested in the formalin assay (Dubuisson and Dennis, 1977). In this assay, mice are injected in one hind paw with dilute formalin, and the behavioral response of hind paw flinches is observed. Quantifying the number of flinches over time thereby provides a measure of pain behavior. Flinches are further divided into those occurring within the first 10 minutes (phase I), which primarily represent an acute pain state, and those that occur

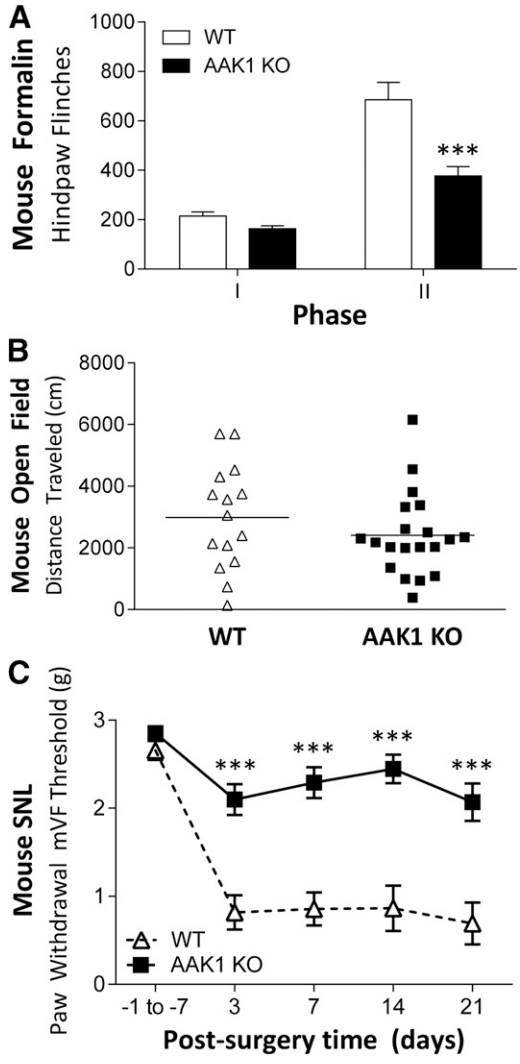

Fig. 1. AAK1 knockout mice have an antinociceptive phenotype in the formalin assay and SNL model. (A) Hind paw flinches in formalin phase I and phase II from wild-type (WT) and AAK1 knockout (AAK1 KO) mice (n = 25–56 per group, male and female mice distributed equally between groups). ***$P < 0.001$ versus WT by two-way repeated measures analysis of variance, followed by Bonferroni's post hoc test. (B) Distance traveled in open field testing of WT (n = 15) and AAK1 KO mice (n = 20). Male and female mice were used and distributed equally between groups. $P = 0.27$ unpaired t test. (C) Mechanical allodynia measured using manual von Frey (mVF) fibers after SNL surgery for WT (n = 15) and AAK1 KO mice (n = 22). Male and female mice were used and distributed equally between groups. ***$P < 0.001$ versus WT by two-way repeated measures analysis of variance, followed by Bonferroni's post hoc test.

between 10 and 60–90 minutes (phase II), which reflect a tonic pain state similar to the relatively long-lasting stimuli in human disease (Dubuisson and Dennis, 1977), such as neuropathic pain. The AAK1 knockout line exhibited a reduced number of flinches in the phase II formalin response (Fig. 1A). This reduced formalin response was not due to suppressed motor function (which can masquerade as lessened pain behavior) because AAK1 knockout mice were indistinguishable from wild-type animals in the open-field assay (Fig. 1B).

The AAK1 knockout mice and wild-type control mice were then tested in a SNL model commonly used to evaluate treatments for neuropathic pain (Kim and Chung, 1992; Ye et al., 2015). In this model, ligation of the L4 and L5 spinal nerves resulted in mechanical allodynia, a painful response to a normally benign tactile stimulus, which developed by 3 days postsurgery and persisted for at least 3 weeks in wild-type mice (Fig. 1C). In contrast to wild-type mice, AAK1 knockout mice did not develop mechanical allodynia following surgery over this same postsurgery period (Fig. 1C). These data were consistent with the lack of persistent pain response in the formalin assay and indicate that AAK1 plays a role in the development of persistent and neuropathic pain states.

A broad phenotypic screen was used to look for other phenotypes in the AAK1 knockout mice (Beltran del Rio et al., 2003). No consistent phenotypes were observed beyond the pain phenotypes described.

A review of the scientific literature indicated that the AAK1 protein was a serine/threonine protein kinase that was implicated in endocytosis (Conner and Schmid, 2002). Endocytosis via clathrin-coated vesicles is a major mechanism to move cell surface proteins to endosomes or lysosomes for recycling or degradation, respectively (reviewed in Traub, 2009). Cell surface proteins are targeted for clathrin-mediated endocytosis by binding the AP-2 adaptor complex. AP-2 consists of four proteins, including the α subunit, $\beta 2$ subunit, $\mu 2$ subunit, and $\sigma 2$ subunit. A variety of sorting signals is used for recognition by the AP-2 complex; one such recognition signal is binding of the $\mu 2$ subunit to the YXXPhi motif in proteins, where X is any amino acid and Phi is a bulky hydrophobic amino acid. The AAK1 kinase phosphorylates threonine 156 of the $\mu 2$ subunit, inducing a conformational change that facilitates binding of YXXPhi motifs and thereby enhances endocytosis (Jackson et al., 2003).

Identification of an AAK1 Inhibitor. The absence of a pain phenotype for AAK1 knockout mice in the SNL model led us to hypothesize that an AAK1 kinase inhibitor might be an effective way to reduce neuropathic pain. To test this hypothesis, selective, small-molecule inhibitors of AAK1 suitable for in vivo studies were identified. In particular, a high-throughput screen and subsequent lead optimization effort led to the identification of a potent and orally available AAK1 inhibitor LP-935509 (Fig. 2A). In an enzyme assay using the human AAK1 kinase domain (amino acids 30–330), LP-935509 inhibited phosphorylation of a peptide derived from the $\mu 2$ protein with an IC_{50} value of 3.3 ± 0.7 nM ($n = 8$) (Supplemental Fig. 1A). To test the activity of LP-935509 in an intact cellular system, the compound was incubated with HEK293 cells overexpressing human AAK1 and the human $\mu 2$ protein. These studies showed that LP-935509 inhibited $\mu 2$ phosphorylation with an IC_{50} value of 2.8 ± 0.4 nM ($n = 26$) (Supplemental Fig. 1B; Table 1). Additional enzymatic studies showed that LP-935509 was competitive with ATP with a Ki of 0.9 nM (Supplemental Fig. 2).

To better understand LP-935509 kinase selectivity, we evaluated the effect of LP-935509 on the kinase activity of the two most closely related kinases, BIKE and GAK (77% and 39% amino acid identity versus AAK1 in the kinase domain,

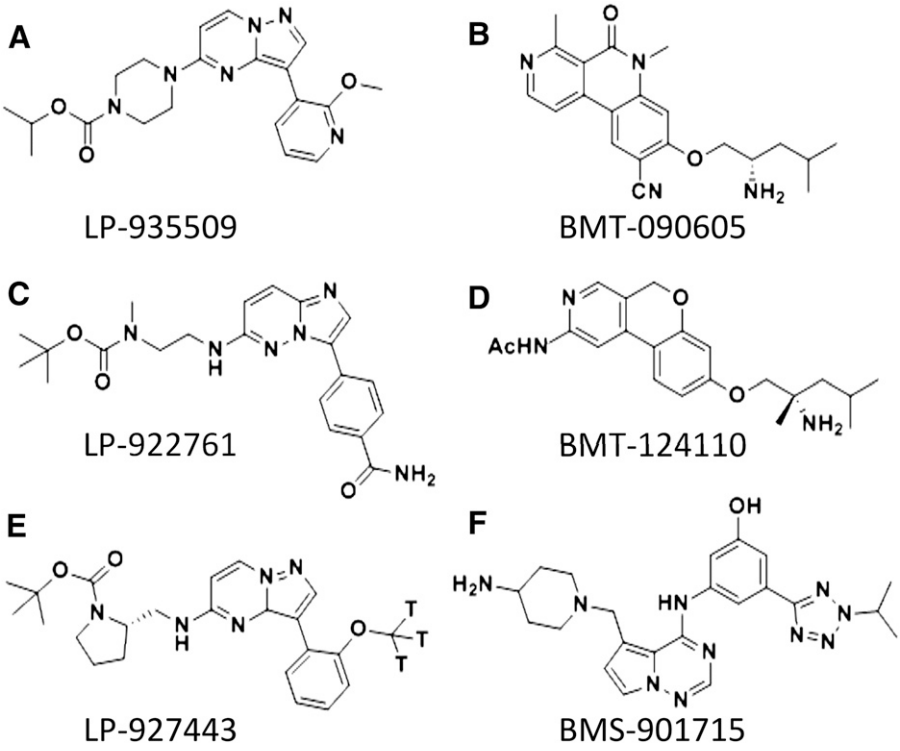

Fig. 2. Chemical structure of AAK1 inhibitors. (A) LP-935509. (B) BMT-090605. (C) LP-922761. (D) BMT-124110 (E) LP-927443. (F) BMS-901715.

TABLE 1
Summary of in vitro properties of AAK1 inhibitors

Assay	LP-935509	LP-922761	BMT-090605	BMT-124110
	Average IC_{50} ± S.E.M. (*n*), nM			
AAK1 enzyme	3.3 ± 0.7 (8)	4.8 (2)	0.6 ± 0.1 (9)	0.9 ± 0.2 (7)
AAK1 binding	3.3 ± 1.5 (4)	3.6 (2)	0.4 ± 0.1 (4)	1.0 (1)
AAK1 cell assay	2.8 ± 0.4 (26)	7.6 ± 0.7 (58)	0.6 ± 0.4 (4)	3.2 ± 1.4 (2)
BIKE enzyme	14 (1)	24 (1)	45 (1)	17 (1)
GAK enzyme	320 ± 40 (2)	NA	60 (1)	99 (1)
μ Opioid receptor binding	>30,000 (1)	15,000 (1)	>30,000 (1)	>30,000 (1)
κ Opioid receptor binding	>30,000 (1)	>30,000 (1)	29,000 (1)	>30,000 (1)
Adrenergic α2A receptor binding	> 30,000 (1)	> 30,000 (1)	> 30,000 (1)	>30,000 (1)
Adrenergic α2C receptor binding	>30,000 (1)	>30,000 (1)	>30,000 (1)	15,000 (1)
Adrenergic α2A functional	>1,000 (4)	NA	>10,000 (4)	NA
Adrenergic α2C functional	>1,000 (3)	NA	>10,000 (3)	NA
GABAa α1 receptor modulator	12,000 (3)	>30,000 (1)	>30,000 (1)	>30,000 (1)
GABAa α2 receptor modulator	12,000 (3)	NA	NA	NA

respectively). These studies showed that LP-935509 was a potent inhibitor of BIKE (IC_{50} = 14 nM) and a modest inhibitor of GAK (IC_{50} = 320 ± 40 nM). To test additional kinases, the ability of 1 μM LP-935509 to inhibit the binding of 389 kinases to an ATP-binding probe was measured. These studies showed that LP-935509 inhibited more than 70% of probe binding to 13 kinases, including BIKE (Supplemental Table 1). None of these other LP-935509–binding kinases have a known connection to pain modulation. In addition, the comparison of kinase profiling data across several of our other AAK1 inhibitors indicated a lack of consistent inhibition at any other kinase aside from BIKE (data not shown).

To further understand the pharmacology of LP-935509, the compound was tested at multiple concentrations in functional or binding assays for 43 receptors, transporters, and enzymes (Supplemental Table 2). LP-935509 was inactive at up to 10 μM in the vast majority of the assays (42 of 43), with the most potent interaction observed for phosphodiesterase 4 (PDE4) (IC_{50} = 8.4 μM). Several receptors and transporters associated with nociception were among those evaluated, including the following: κ and μ opioid receptors (binding IC_{50} > 30 μM), NET (IC_{50} = 22 μM), SERT (IC_{50} > 30 μM), α2A and α2C adrenergic receptors (binding IC_{50} > 30 μM), and positive modulation of γ-aminobutyric acid (GABA)a α1– and GABAa α2–containing channels (EC_{50} = 12 μM and 12 μM, respectively).

Taken together, these studies show that LP-935509 is a potent and selective AAK1 kinase inhibitor. Although the inhibition of BIKE could contribute to nociception, it is unlikely that other pharmacologic activities of LP-935509 are relevant for nociception.

An AAK1 Inhibitor Recapitulates the AAK1 Knockout Antinociceptive Phenotype in Mice. To facilitate the use of LP-935509 in mouse behavioral studies, the pharmacokinetic properties of LP-935509 in mice were quantified. For these studies, four mice were dosed with LP-935509 either i.v. (1 mg/kg) or orally (10 mg/kg). Blood samples were taken over a 24-hour period, and LP-935509 plasma levels were determined (Supplemental Fig. 4). PK parameters were fit to standard PK models. This analysis showed that LP-935509 had 100% oral bioavailability and a plasma half life of 3.6 hours. The Cmax for the 10 mg/kg oral dose was 5.2 μM at 0.5-hour postdose. In addition, LP-935509 had a plasma-free fraction of 2.6% in mice. Brain drug levels exceeded plasma drug levels with a brain/plasma drug ratio typically between 3 and 4, showing that LP-935509 was highly brain-penetrant. Based on these data, LP-935509 was considered a suitable compound for oral delivery to evaluate the effect of AAK1 inhibition on nociception.

The effect of LP-935509 on the formalin phase II responses was tested to determine whether a small-molecule AAK1 inhibitor could recapitulate the AAK1 knockout phenotype. These studies showed that oral delivery of LP-935509 caused a dose-dependent reduction in phase II paw flinches that was significantly lower than the vehicle-treated animals (Fig. 3A). In particular, 30 mg/kg and 60 mg/kg LP-935509 caused a robust reduction in pain behavior similar to a high dose of gabapentin (200 mg/kg) (Fig. 3A). LP-935509 was then tested in the mouse SNL model, and oral delivery exhibited a dose-dependent reversal of the mechanical allodynia, with 60 mg/kg-treated mice displaying behavioral responses to tactile stimuli similar to a presurgery mouse by 120 minutes postdose (Fig. 3B). As expected, gabapentin (200 mg/kg) also reduced mechanical allodynia in this assay. Unlike high doses of gabapentin, which are known to cause motor impairment and sedation, the effects of LP-935509 in the mouse formalin and SNL assays were not due to decreased locomotor activity as mice treated orally with the same doses of LP-935509 were indistinguishable from vehicle-treated animals in the open-field assay (Fig. 3C).

LP-935509 plasma and brain drug levels were measured in satellite animals during the mouse formalin, SNL, and open field tests (Supplemental Table 3). These measurements showed that brain drug levels exceeded plasma drug levels, showing that LP-935509 is highly brain-penetrant and suggesting that LP-935509 broadly distributed to tissues. For the mouse formalin and SNL assays (Fig. 3, A and B), LP-935509 reversed approximately half of the behavioral deficit at 10 mg/kg, which corresponded to free drug levels in satellite animals at 30–120 minutes that were about 30-fold higher than the cellular IC_{50} value of 2.7 nM (Supplemental Table 3).

To better understand the relationship of LP-935509 efficacy to exposure, the compound was dosed in the SNL mice at 3, 10, and 30 mg/kg, and testing was carried out at several times, concluding with a final time of 24 hours (Fig. 4). LP-935509 plasma exposures were determined using satellite mice. Efficacy peaked by 2 hours, declined by 5 hours, and was absent by 24 hours. Total plasma exposures were highest at the 30 minutes and declined by 24 hours to less than 2% of the peak exposure. These data suggest that efficacy is correlated

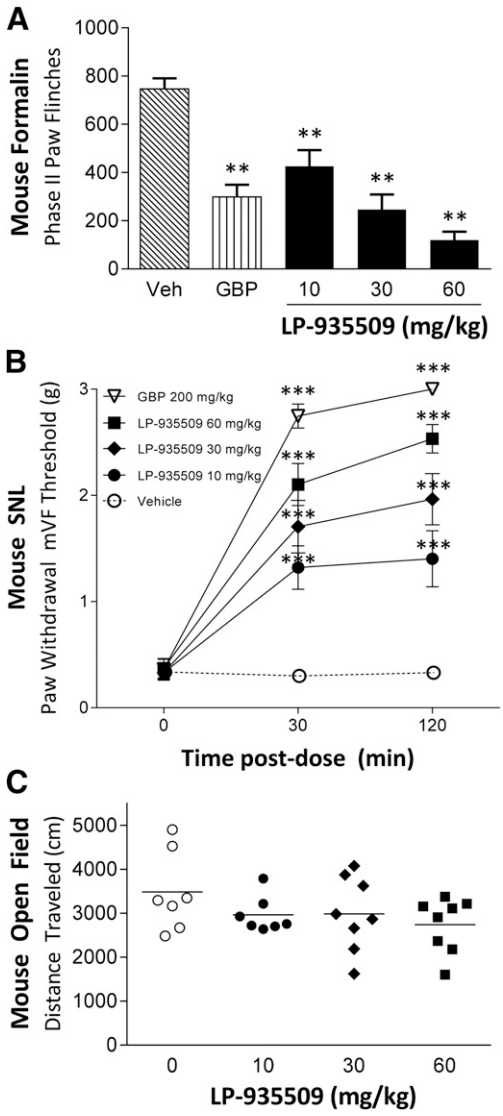

Fig. 3. AAK1 inhibitor LP-935509 recapitulates the knockout phenotype in mice. (A) Mouse phase II formalin responses after oral vehicle, gabapentin (GBP) (200 mg/kg), or LP-935509 (10, 30, or 60 mg/kg) (n = 8–10 male mice per group). $^{**}P < 0.01$ versus Veh by one-way analysis of variance, followed by Dunnett's t test. (B) Mechanical allodynia over time postdose [doses as in (A)] in mice with SNL injury after oral vehicle, GBP, or LP-935509 (n = 9–13 male mice per group). $^{***}P < 0.001$ versus vehicle by repeated measures analysis of variance, followed by Dunnett's t test. (C) Open field locomotor activity of mice at 30 minutes after oral [doses as in (A)] vehicle, GBP, or LP-935509 (n = 7 male mice per group). $P = 0.27$ by one-way analysis of variance.

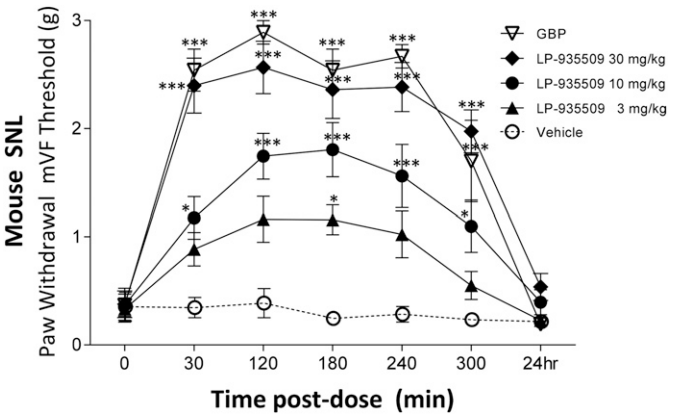

Fig. 4. AAK1 inhibitor LP-935509 efficacy in SNL model follows plasma exposure. Mouse SNL mechanical allodynia responses after oral vehicle, gabapentin (GBP) (200 mg/kg), or LP-935509 (3, 10, or 30 mg/kg) (n = 4–7 male mice per group). $^{*}P < 0.05$ and $^{***}P < 0.001$ versus vehicle by repeated measures analysis of variance, followed by Dunnett's t test.

with drug levels with efficacy delayed approximately ~2–3 hours from exposure.

LP-935509 was then evaluated in a 5-day repeat dosing study in SNL mice to test for tolerance (Fig. 5). Mice received two daily doses of 3, 10, or 30 mg/kg per day for 5 days. Efficacy was consistent at each dose level from day to day, revealing no evidence for tolerance or potentiation with repeated dosing. Exposures and efficacy levels were consistent with previous studies. Plasma exposures indicated compound levels were not altered by repeated dosing relative to single doses (Supplemental Table 6).

Given the potent inhibition of BIKE activity and the absence of data regarding the impact of BIKE inhibition on neuropathic pain, we generated BIKE knockout mice. SNL surgery of BIKE knockout mice revealed that these mice developed 30% less allodynia after SNL surgery than wild-type mice (Supplemental Fig. 3). Although the loss of BIKE was not as impactful as AAK1 loss on mechanical allodynia in the SNL model, BIKE inhibition may contribute to antinociception from LP-935509.

An AAK1 Inhibitor Is Antinociceptive in Rat Models of Neuropathic Pain but Not Acute Pain. To facilitate the use of LP-935509 in rat behavioral studies, the pharmacokinetic properties of LP-935509 in rats were quantified. For these studies, three rats were dosed i.v. with 2 mg/kg LP-935509 and three rats were dosed orally with 10 mg/kg LP-935509. Blood samples were taken 10 times over a 24-hour period, and LP-935509 plasma levels were determined (Supplemental Fig. 5). Pharmacokinetic parameters were determined by noncompartmental analysis. This analysis showed that LP-935509 had 50% oral bioavailability and a plasma half life of 4.0 hours. Brain drug levels exceeded plasma drug levels, with a brain/plasma drug ratio of 2.3 showing that LP-935509 was highly brain-penetrant. The Cmax for the 10 mg/kg oral dose was 3.1 μM at 1.3 hours postdose. In addition, LP-935509 had a plasma-free fraction of 2.6% in rat. Based on these data, LP-935509 was considered a suitable compound for oral delivery to evaluate the effect of AAK1 inhibition on nociception.

The effect of LP-935509 on antinociception was further explored in rats because this species is commonly used to evaluate novel antinociceptive agents. LP-935509 was first tested in the CCI model. In this assay, the sciatic nerve is loosely ligated, which creates a neuropathic state within a few days after surgery, which lasts for several months (Bennett and Xie, 1988). In CCI animals, oral LP-935509 caused a dose-dependent reversal of thermal hyperalgesia (Fig. 6A), cold allodynia (Fig. 6B), mechanical allodynia (Fig. 6C), and mechanical hyperalgesia (Fig. 6D). In particular, LP-935509 completely reversed thermal hyperalgesia and mechanical allodynia at 10 and 30 mg/kg, with most assays showing significant antinociceptive activity at lower doses (ranging from 0.3 mg/kg to 3 mg/kg). The maximal reversal of the pain response was similar to that obtained by a high-dose gabapentin. The effects of LP-935509 on the CCI pain

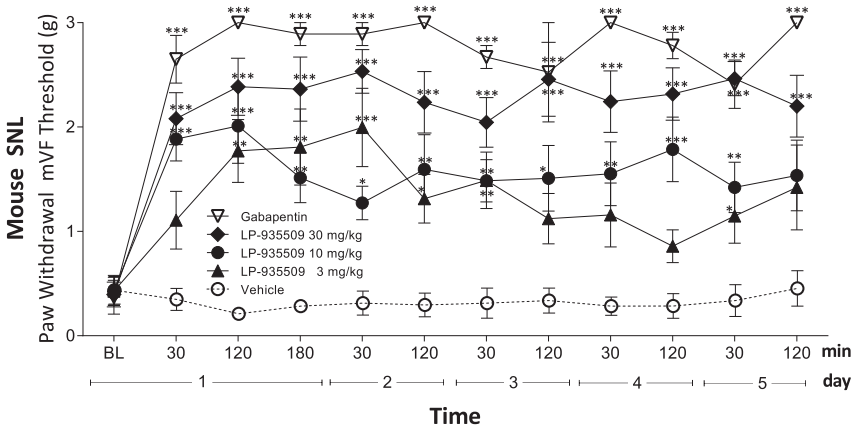

Fig. 5. AAK1 inhibitor LP-935509 efficacy in SNL model does not change with repeat dosing. Mouse SNL mechanical allodynia responses with twice-daily dosing over 5 consecutive days with oral vehicle, gabapentin (200 mg/kg), or LP-935509 (3, 10, or 30 mg/kg) (n = 4–7 male mice per group). $^{*}P < 0.05$, $^{**}P < 0.01$, and $^{***}P < 0.001$ versus vehicle by repeated measures analysis of variance, followed by Dunnett's t test.

responses were not due to reduced functional motor abilities as oral LP-935509–treated animals were indistinguishable from vehicle-treated animals in the rat accelerating rotarod assay (Fig. 6E). In contrast, the 100 mg/kg dose of gabapentin used in these studies caused motoric impairment, which could confound measurement of the pain response. In our studies, gabapentin effects on pain behavioral measurements and impairment in rat rotarod were not well separated, with impairment in rotarod occurring at doses as low as 30 mg/kg, the minimal efficacious dose (Supplemental Fig. 6).

LP-935509 was then tested in the STZ model of diabetic peripheral neuropathy (Courteix et al., 1993). In this model, rats are administered STZ (50 mg/kg), which kills insulin-producing pancreatic β islet cells, thereby creating a diabetic state that is accompanied by allodynia and hyperalgesia, which increase progressively over 2–4 weeks. LP-935509 caused a dose-dependent reversal of mechanical allodynia in the STZ-treated rats to control levels (Fig. 6F). The antinociceptive efficacy observed at 3 mg/kg to 30 mg/kg was similar to high-dose (100 mg/kg) gabapentin.

LP-935509 plasma and brain drug levels were measured (Supplemental Table 3) after the behavioral studies in CCI and STZ rats (Fig. 6, A–F). In these studies, LP-935509 reversed the behavioral deficits, with ED_{50} values ranging from 2 mg/kg to 10 mg/kg, which corresponded to plasma drug levels at 180–240 minutes that were about eightfold higher than the cellular IC_{50} value of 2.7 nM (Supplemental Table 3).

LP-935509 was then tested in assays for acute pain, including the hot-plate and tail-flick assays. In the hot-plate assay, animals are placed in a chamber on a hot (55°C) temperature-controlled surface, and the time to exhibit a hind limb response (e.g., licking or dancing) or a jump-escape response (i.e., leaping up onto the top edge of the enclosing chamber) is recorded (Woolfe and MacDonald, 1944). The time between placement of the animal into the test chamber and the display of a response is recorded as the hind limb response latency. To prevent tissue damage, animals that fail to exhibit a hind limb response by the cutoff time of 30 seconds are removed from the test chamber. In the tail-flick assay, a radiant heat source is positioned above the tail and directed through an aperture to stimulate the tail (D'Amour and Smith, 1941). The time between lamp onset and the response of flicking the tail to escape the thermal stimulus is recorded as tail-flick latency. To prevent tissue damage, animals that fail to respond to the radiant heat by the cutoff time of 10 seconds are removed from the stimulus. In both the hot-plate and tail-flick assays, 30 mg/kg oral LP-935509 did not affect the pain response, whereas 5 mg/kg morphine was highly analgesic (Fig. 6, G and H). The 30 mg/kg LP-935509 dose is maximally efficacious in our neuropathic pain models. Taken together, these results show that LP-935509 reduces neuropathic pain behaviors in mice and rats but does not affect acute pain perception.

AAK1 Inhibitors Cause Antinociception by Inhibiting AAK1 in the Spinal Cord. AAK1 is broadly distributed throughout the body, and LP-935509 is a highly permeable compound that is widely distributed to tissues. Hence, neither the target location nor the compound distribution is informative as to the location of the relevant pool of AAK1 for antinociception. To help address this question, LP-922761 was identified (Fig. 2C). LP-922761 is a potent and selective AAK1 inhibitor with an in vitro IC_{50} value of 4.8 ± 0.8 nM and a cellular IC_{50} value of 7.6 ± 0.7 nM (Table 1). Whereas LP-935509 has a brain to plasma drug level ratio >2, LP-922761 had a brain to plasma ratio of 0.007, indicating that LP-922761 was essentially restricted to the peripheral compartment. When oral LP-927761 (60 mg/kg) was tested in the mouse for relief of mechanical allodynia following SNL surgery, the compound was not antinociceptive (Fig. 7A), whereas gabapentin (200 mg/kg) showed significant activity in the same assay. The inactivity of oral LP-922761 was not due to inadequate drug exposure because drug levels at the time of behavioral testing exceeded those of LP-935509 both with respect to total (>11 μM) and free drug levels (>1200 nM) (Supplemental Table 3). These results with LP-922761 show that AAK1 inhibitors must cross the blood-brain barrier to be antinociceptive.

We next investigated intrathecal injection of an AAK1 inhibitor to determine whether AAK1 inhibitors could act at the level of the spinal cord. LP-935509 was not suitable for these studies due to poor aqueous solubility. Instead, we identified BMT-090605 (Fig. 2B) as a potent, selective AAK1 inhibitor (cellular IC_{50} = 0.63 ± 0.39 nM) with suitable physiochemical properties for intrathecal injection (Table 1). BMT-090605 (0.3–3 μg/rat) was delivered intrathecally at lumbar level L5/L6 to CCI animals. Behavioral evaluation of these animals showed that spinal delivery of BMT-090605 caused a dose-dependent reduction in thermal hyperalgesia (Fig. 7B). The high dose of BMT-090605 (3 μg/rat) showed efficacy comparable to intrathecal clonidine (3 μg/rat). Exposure measurements from this study indicated that brain and plasma levels of BMT-090605 were <4 nM, whereas

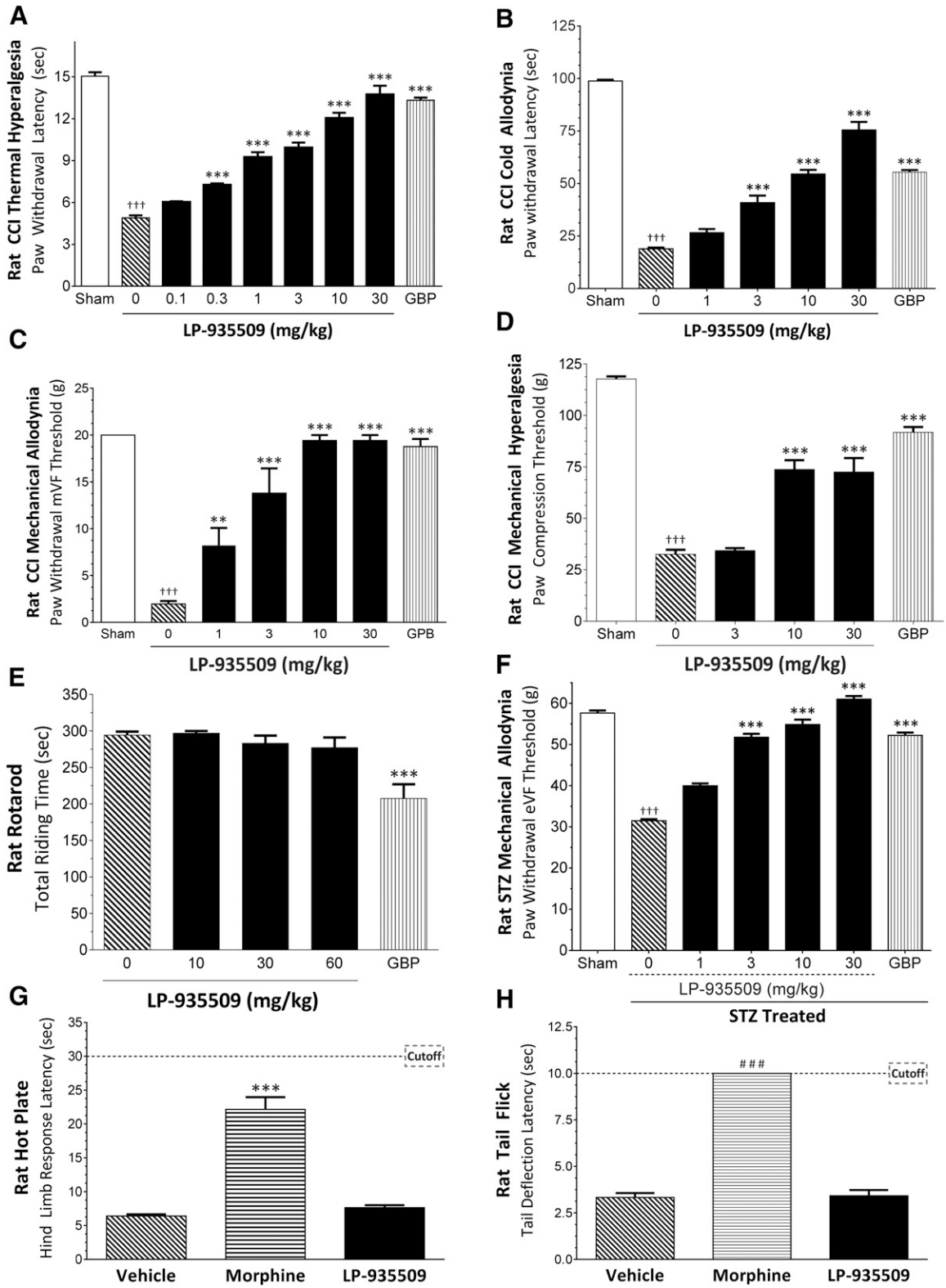

Fig. 6. AAK1 inhibitor LP-935509 is antinociceptive in multiple rat models of neuropathic pain, but not acute pain (A–D). CCI-operated rats were tested at 3 hours after oral vehicle (0), LP-935509 (at indicated doses), or gabapentin (GBP; 100 mg/kg) in assays of (A) thermal hyperalgesia, (B) cold allodynia, (C) mechanical allodynia using Manual von Frey, or (D) mechanical hyperalgesia (n = 7–8 male rats per group). For comparison, sham-operated animals (Sham) are included. (E) Naive rats were testing in the accelerating rotarod assay, dosed as in Fig. 4, (n = 5–10 male rats per group). (F) STZ-injured rats were tested for mechanical allodynia, dosed as in Fig. 4, (n = 7–8 male rats per group). For comparison, sham-injected animals (Sham) are included. (G and H) Naive rats were tested in assays of acute pain, including the following: (G) hot plate and (H) tail flick at 1.5 hours after LP-935509 (30 mg/kg, Per Os po) or 0.5 hour after morphine (5 mg/kg, s.c.) (n = 7–8 male rats per group). $^{***}P < 0.001$ versus vehicle, or $^{\dagger\dagger\dagger}P < 0.001$ versus sham controls by one-way analysis of variance, followed by Bonferroni's post hoc test; $^{\#\#\#}P < 0.001$ versus vehicle by paired t test.

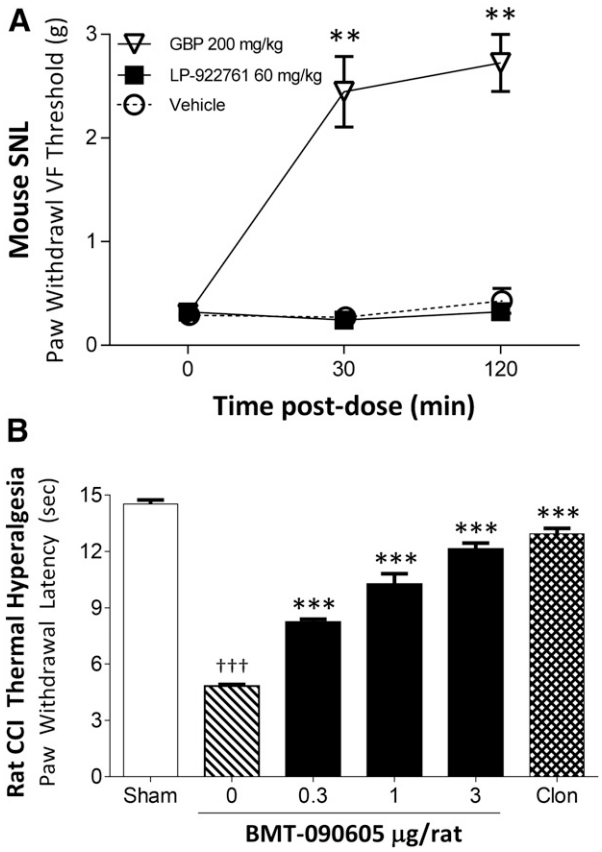

Fig. 7. AAK1 inhibitors cause antinociception by inhibiting AAK1 in the spinal cord. (A) Mice with SNL injury were tested for thermal hyperalgesia 2 hours after oral vehicle, LP-922761 (poorly brain-penetrant AAK1 inhibitor), or gabapentin (GBP) at indicated doses (n = 7–8 male rats per group). (B) Rats with CCI surgery were tested for thermal hyperalgesia 15 minutes after intrathecal vehicle (0), BMT-090605 (0.3–3 μg/rat), or clonidine (Clon, 3 μg) (n = 7–8 male rats per group). For comparison, sham-operated animals (Sham) are included. $^{**}P < 0.01$ $^{***}P < 0.001$ versus vehicle/0, $\dagger\dagger\dagger P < 0.001$ versus Sham by one-way analysis of variance, followed by Bonferroni's post hoc test.

measurable levels (90–317 nM) were observed in lumbar spinal cord (Supplemental Table 4). Total compound levels are >100-fold the cellular IC_{50} (Supplemental Table 3) at the lowest dose. In addition, there is most likely a compound gradient in the tissue with higher exposures in the pain-related dorsal horn. These data show that AAK1 inhibition localized to the spinal cord is sufficient for antinociceptive efficacy in CCI rats.

AAK1 Inhibitors Decrease Neural Activity in Pain-Related Circuits at the Spinal Level. Rats with chronic constriction injury have increased spontaneous activity in the dorsal horn neurons of the spinal cord (Laird and Bennett, 1993; Liu and Walker, 2006). To test the effect of AAK1 inhibitors on this activity, we developed methods to record spontaneous activities from the spinal cord in anesthetized rats. In this assay, spontaneous action potential spikes from single neurons in the lamina V of the spinal cord were isolated and recorded extracellularly, and the response of the spike frequency to compound treatment was tested. These studies showed that rats that had undergone the CCI procedure had elevated spontaneous activity at an average of 23.3 ± 2.4 Hz in the spinal dorsal horn neurons in comparison with 1.2 ± 0.3 Hz in rats that had not undergone the CCI procedure. The effect of LP-935509 on this increased spontaneous activity was then tested using i.v. delivery to more precisely control the onset of drug action upon electrophysiological responses. These studies showed that LP-935509 reduced CCI-induced increases in spontaneous activity at 3 mg/kg (Fig. 8A). LP-935509 effects on spontaneous firing began within 8 minutes of infusion and achieved near-complete blockade of injury-induced activity by 10 minutes. Blockade persisted for another 10 minutes and then showed a partial reversal at later times consistent with an expected reduction in drug levels. These studies were extended to multiple doses showing that LP-935509 (0.3–3 mg/kg) caused a dose-dependent reduction in spontaneous activity in CCI animals (Fig. 8B). LP-935509 was effective in the majority of neurons (7 of 10) in this study, suggesting that AAK1 antinociception is restricted to a subset of neurons that are activated by CCI. To determine whether AAK1 antinociception required the engagement of descending pain pathways, the spinal cord of CCI rats was transected at T8–T9, and the effect of LP-935509 on spontaneous activity was tested. AAK1 inhibition continued to produce a suppression of injury-induced activity in spinally transected animals and also achieved a near-complete blockade lasting for several minutes (Fig. 8C). Comparing these two experiments showed that spinal cord transection did not affect the AAK1 inhibition–induced reduction of spontaneous activity in CCI rats. The effect of LP-935509 (1 mg/kg) was the same regardless of whether the spinal cord was intact (Fig. 6B) or transected (Fig. 8D). These data indicate that intact descending pathways are not required for AAK1 inhibitor effects on spontaneous firing and suggest that either peripheral or local spinal action is sufficient to account for the observed reduction in spontaneous activity in CCI rats.

Windup is another electrophysiologic measure that is affected by drugs that are used to treat neuropathic pain (Arendt-Nielsen et al., 2011). In the animal assay of windup, a train of 16 electrical stimuli (2 ms, 0.5 Hz, 2 mA) was delivered transcutaneously to the hind paw to activate C-fiber–mediated windup activity of the wide-dynamic range neurons in the spinal dorsal horn of naive rats, and the effect of LP-935509 on the windup activity was then examined. These results showed that 1 and 3 mg/kg LP-935509 administered i.v. reduced windup activity in a dose-dependent manner (Fig. 8, E and F). In this study, 9 of 12 animals significantly responded to LP-935509, suggesting that a majority, but not all, neurons in the pain circuit are regulated by AAK1. To determine whether the AAK1 inhibitor effects on windup were operating in the spinal cord, BMT-124110 (cellular IC_{50} = 3.2 ± 1.4 nM) (Fig. 2D) was added directly onto the spinal cord by microiontophoresis, leading to reduction in windup-induced activity in 10 of 14 animals (Fig. 8, G and H). BMT-124110 is structurally similar to BMT-090605, but had the appropriate combination of solubility and charge required for microiontophoresis. In this procedure, double-barrel microelectrodes were used to record neuronal activity and to apply BMT-124110 by microiontophoresis. Taken together, these results indicate that AAK1 antinociception results from inhibition of pain circuits in the spinal cord.

α2 Adrenergic Antagonist Blocks AAK1 Inhibitor–Induced Antinociception and Inhibition of Spontaneous Neural Activity. To further probe the mechanism of AAK1 inhibitor antinociception, chemical inhibitors of known pain pathways were tested to determine whether they blocked

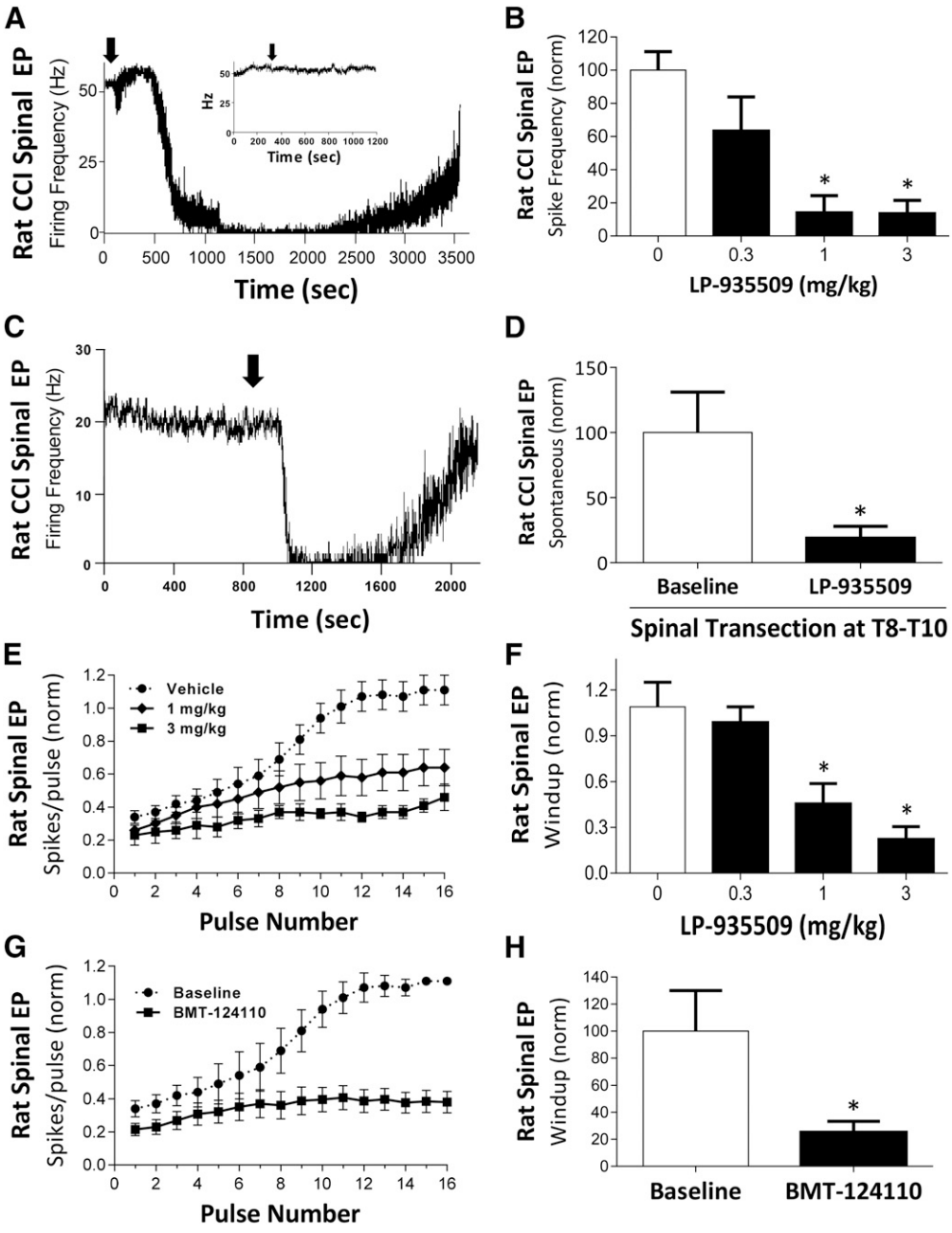

Fig. 8. AAK1 inhibitors decrease neural activity in pain-related circuits. (A) CCI rat spontaneous activity over time of a single spinal dorsal horn neuron showing inhibition by LP-935509 (1 mg/kg, i.v.). Arrow indicates time of LP-935509 injection (inset shows response to vehicle). (B) Dose-dependent inhibition by LP-935509 (0.3–3 mg/kg, i.v.) on spontaneous activity of spinal dorsal horn neurons in CCI male rats (responders, n = 3/4 at 1 mg/kg, n = 4/6 at 3 mg/kg). *$P < 0.05$ versus vehicle (0) by one-way analysis of variance, followed by Dunnett's t test. (C) Absence of effect of thoracic T8–T10 transection on LP-935509 (1 mg/kg, i.v.) inhibition of spontaneous activity over time in a single spinal dorsal horn neuron of a CCI male rat (arrow indicates time of injection). (D) Effect of LP-935509 (1 mg/kg, i.v.) on normalized spontaneous activity of CCI male rats (n = 4) with thoracic T8–10 transection. *$P < 0.05$ versus baseline by unpaired t test. (E) Naive wide-dynamic range neuron spikes evoked by hind limb repetitive electrical stimulation (16 pulses, 2 ms, 2.0 mA) with effect of systemic vehicle or LP-935509 (1–3 mg/kg, i.v.) across pulses (n = 4–8 male rats per group). (F) Systemic inhibition by LP-935509 (0.3–3 mg/kg, i.v.) of electrically evoked windup in spinal wide-dynamic range neurons from naive male rats (responders, n = 5/8 at 1 mg/kg, n = 4/4 at 3 mg/kg). *$P < 0.05$ versus vehicle (0) by one-way analysis of variance, followed by Dunnett's t test. (G) Naive rat spinal wide-dynamic range neuron spikes across pulses (as in Fig. 6E) with effect of microiontophoretically-applied BMT-124110 (30 mM, pH 4, +10–30 nA, 3 minutes) (n = 10 male rats per group). (H) Spinal inhibition by BMT-124110 (as in Fig. 6G) of electrically evoked windup in dorsal horn wide-dynamic range neurons from naive male rats (responders, n = 10/14). *$P < 0.05$ by unpaired t test.

AAK1 inhibitor effects. We first tested the effect of naloxone, an inhibitor of opioid signaling. These studies showed that naloxone did not affect the ability of LP-935509 to reduce mechanical allodynia in the STZ model of diabetic pain (Fig. 9A). Naloxone was pharmacologically active in these experiments because naloxone fully inhibited the activity of the opioid agonist morphine. These data indicate that AAK1 inhibitors do not work through or require opioid signaling. In a separate study, we evaluated potential interactions with the noradrenergic pain-regulating system. Yohimbine, an inhibitor of α2 adrenergic

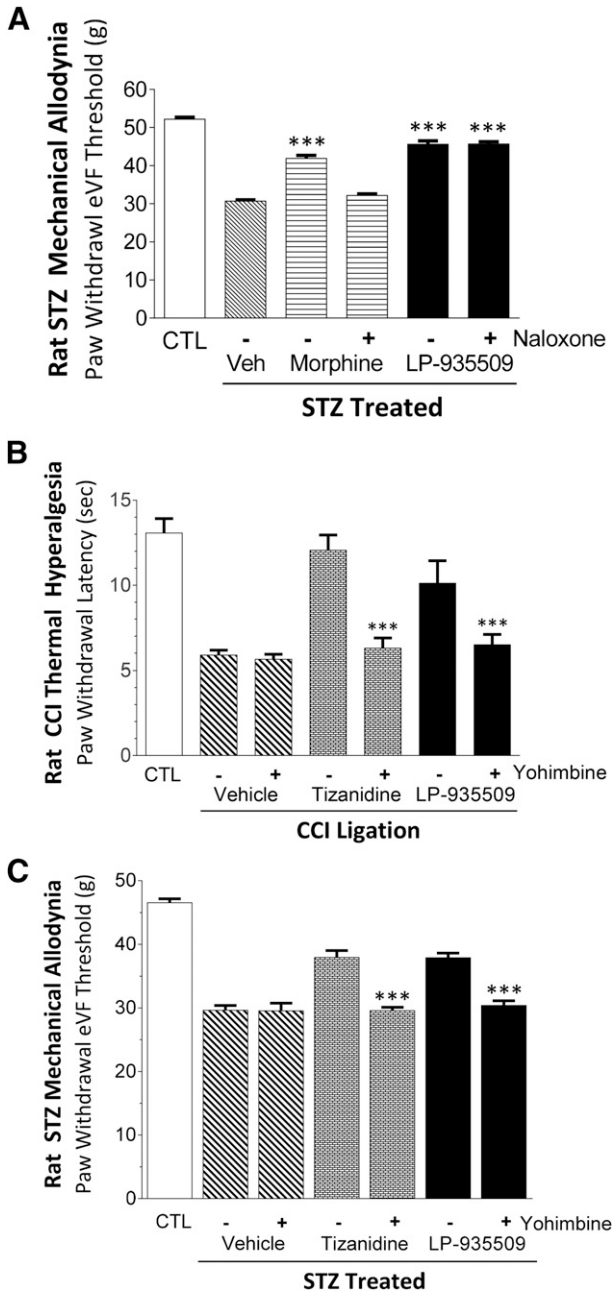

Fig. 9. α2 adrenergic antagonist blocks AAK1 inhibition–induced antinociception in CCI and STZ rats. (A) STZ-treated rats were tested for mechanical allodynia using electronic von Frey 1.5 hours after vehicle (per os), LP-935509 (30 mg/kg, per os), or morphine (3 mg/kg, s.c.) delivered in the presence (+) or absence (−) of naloxone (1 mg/kg, s.c.) given 30 minutes prior to the other agents (n = 8 male rats per group). For comparison, sham-treated (CTL) animals are included. ***$P < 0.001$ versus vehicle by one-way analysis of variance, followed by Bonferroni's post hoc test. (B) CCI-operated rats were tested for thermal hyperalgesia 30 minutes after tizanidine (1 mg/kg, i.p.), or 1.5 hours after either vehicle (per os) or LP-935509 (30 mg/kg, po) all delivered in the presence (+) or absence (−) of yohimbine (1 mg/kg, i.p.) given 100 minutes before testing (n = 6–11 male rats per group). CTL as in (A). ***$P < 0.001$ versus (−) yohimbine pair by one-way analysis of variance, followed by Bonferroni's post hoc test. (C) STZ-treated rats were tested for mechanical allodynia with CTL and dosing as in (B) (n = 8 male rats per group). ***$P < 0.001$ versus (−) yohimbine as in (B).

receptors, prevented LP-935509 reductions in CCI thermal hyperalgesia and STZ mechanical allodynia (Fig. 9, B and C). As expected, yohimbine also blocked the antinociceptive effects of tizanidine, an α2 adrenergic agonist, in these thermal and mechanical hyperalgesia assays. LP-935509 exposures did not differ significantly with and without yohimbine cotreatment (Supplemental Table 5). Similar data were generated with the AAK1 inhibitor BMT-090605 (data not shown), indicating the interaction of AAK1 and α2 adrenergic pathways was a general feature of AAK1 inhibition. LP-935509 and BMT-090605 do not alter adrenergic ligand binding to human α2A and α2C receptors and showed little or no agonist activity in recombinant cellular α2A and α2C cellular assays (Table 1). These data suggest that these AAK1 inhibitors are not acting directly on α2 adrenergic receptors.

Similar pharmacologic effects were also seen in whole-animal in vivo electrophysiology studies of CCI rats. The LP-935509–induced reduction in CCI-evoked spontaneous activity (Fig. 10A, top trace) was blocked by pretreatment with yohimbine (Fig. 10A, bottom trace). Yohimbine alone was without significant effect, but fully prevented the reduction in spontaneous activity of spinal cord dorsal horn neurons shown by LP-935509 (Fig. 8B). Thus, in both behavioral (Fig. 9B) and electrophysiological (Fig. 10) assays, yohimbine pretreatment prevented the beneficial effects of LP-935509 in CCI rats.

Discussion

This study identified AAK1 as a novel target for antinociception using the formalin assay to screen knockout mice. The ability of AAK1 knockouts to significantly reduce formalin phase II responses was extended to show that AAK1 knockouts also fail to develop mechanical allodynia in the mouse SNL model of neuropathic pain. AAK1 knockout mice exhibited no other phenotypes in a broad phenotypic screen, suggesting AAK1 is a promising target for reducing neuropathic pain while avoiding other mechanism-based toxicities. Based on these findings, selective and potent small-molecule inhibitors of AAK1 kinase activity were discovered. These AAK1 inhibitors dose-dependently reduced nociceptive behavioral responses in multiple rodent assays of neuropathic pain, inhibited spontaneous neuronal activity in the spinal cord due to chronic constriction injury, and blocked the development of windup normally elicited by repeated electrical pulses. The effects in behavioral assays of neuropathic pain were present across a variety of stimulus modalities (thermal, mechanical, chemical, electrical) without confounding motor deficits. Multiple-day dosing of AAK1 inhibitor in the SNL model showed no evidence of tolerance.

AAK1 inhibition did not alter acute nociception in the phase I formalin test, hot-plate assay, and tail-flick assays, suggesting that AAK1 inhibition causes a selective antineuropathic effect while leaving normal nociception intact. The behavioral impact of AAK1 inhibitors was mirrored electrophysiologically in the selective dampening by AAK1 inhibition of spontaneous neuronal activity following CCI injury, while preserving some ongoing activity like that observed in non-injured control animals. Similarly, the peak effect of AAK1 inhibition observed in normal animals in the windup assay did not drop below the baseline activity observed in the first pulse.

The blockade of AAK1 inhibitor–induced antinociception and electrophysiologic effects by α2-adrenergic inhibitors links AAK1 inhibition to a major inhibitory pain pathway

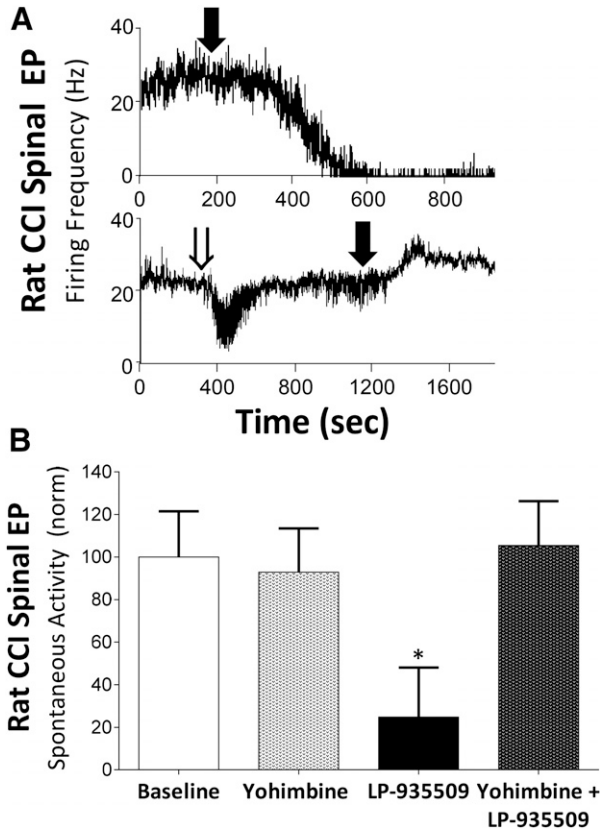

Fig. 10. α2 adrenergic antagonist blocks AAK1 inhibition–induced reduction in spontaneous neuronal activity in CCI rats. (A) CCI rat spontaneous activity time course of two individual spinal dorsal horn neurons treated with LP-935509 (1 mg/kg, i.v.; filled arrow) without (top trace) or with (bottom trace) pretreatment of yohimbine (0.3 mg/kg, i.v.; open arrow). (B) CCI rat group data for spontaneous activity with design and dosing as in (A) plus baseline and yohimbine controls (n = 6–8 male rats per group). *$P < 0.05$ versus baseline by one-way analysis of variance, followed by Dunnett's t test.

used by endogenous and exogenous antinociceptives. In particular, the most commonly prescribed medications for neuropathic pain, gabapentinoids, tryclic antidepressants, and SNRIs, act (at least in part) through the α2-adrenergic pathway (Fairbanks et al., 2009). In addition to linking AAK1 to the α2-adrenergic pathway, our studies provide clues to the antinociceptive mechanism of AAK1 inhibitors. The inhibitory effects of AAK1 inhibitors in spinal cord preparations and failure of spinal transection to reduce AAK1 inhibitor suppression of spontaneous activity suggest that AAK1 inhibition acts at a spinal level to reduce ascending pain signals. This may involve modification of synaptic transmission from dorsal root ganglion cell terminals in the dorsal horn or even altering local circuits within the dorsal horn. Attempts to further define the cellular site of action using spinal slice electrophysiology were hampered by the paucity of tools to precisely define and modulate specific neuronal populations. AAK1 mRNA is expressed in the many brain areas as shown in the Allen Brain Atlas, and AAK1 protein immunoreactivity is detected in the spinal cord (Shi et al., 2014). Thus, although we have focused on the spinal cord site of action as sufficient for AAK1 inhibitor antinociceptive effects, we cannot rule out a possible supraspinal contribution with systemic administration.

Given the role for AAK1 in endocytosis, we hypothesized that reduced endocytosis of a key cell surface protein(s) involved in transmitting pain signals could explain AAK1 antinociception. Based on this hypothesis, we searched for proteins with the YXXPhi motif that might have a known function that could explain the role of AAK1 in neuropathic pain. Whereas neither α2A nor α2C adrenergic receptors contained this motif, $GABA_A$ γ2 protein contained this motif. The $GABA_A$ γ2 protein is a component of $GABA_A$ channels that contain α, β, and γ subunits. Activation of these channels by GABA increases chloride conductance, thereby typically decreasing membrane potential and action potentials. The importance of endocytosis for regulating surface levels of μ2-containing $GABA_A$ channels is supported by two experiments. First, a peptide inhibitor of $GABA_A$ Cl channel–μ2 binding increased $GABA_A$–dependent mini-inhibitory postsynaptic currents in striatal neurons (Kittler et al., 2008). Second, a naturally occurring $GABA_A$ γ2 protein mutation (R43Q) found in a patient with childhood epilepsy increased cell surface levels by decreasing endocytosis (Chaumont et al., 2013). The importance of μ2-dependent endocytosis on $GABA_A$ Cl channel function is particularly interesting given the role of $GABA_A$ Cl channel in nociception. In particular, multiple studies show that GABA agonists are antinociceptive in preclinical models of neuropathic pain but not human pain, perhaps due to dose-limiting sedation or tolerance (reviewed in McCarson and Enna, 2014; Zeilhofer et al., 2015). The antinociceptive activity of $GABA_A$ agonists has been localized to the spinal cord, where $GABA_A$ receptors are found on primary sensory neurons and intrinsic dorsal horn neurons. Taken together, the antinociceptive effects of increasing GABA activity and its dependence on μ2 endocytosis make $GABA_A$ channels an appealing hypothetical target of AAK1 antinociceptive effects.

Although we have focused on the more studied role of AAK1 in modulating cargo capture in clathrin-coated endocytosis through μ2 phosphorylation, there are several other AAK1-related activities that have been reported. One group identified AAK1 (S635) as a substrate for the kinase NDR1/2 and showed that AAK1 plays a role in dendritic branching and length in cultured rat hippocampal neurons (Ultanir et al., 2012). The relevance of these observations for the role of AAK1 in neuropathic pain is unclear because these dendritic effects took days to manifest, whereas AAK1 antinociception occurred within minutes. Another group reported that AAK1 knockdown or inhibition leads to ErbB4 accumulation in PC12 cells and potentiates Nrg1-ErbB4–mediated neurite outgrowth (Kuai et al., 2011). Interestingly, intrathecal injection of the Nrg1 peptide was recently found to be antinociceptive in the SNL model (Wang et al., 2014). AAK1 has also been reported as a positive regulator of the notch pathway (Gupta-Rossi et al., 2011), which has been linked to pain. In particular, Notch inhibition with a γ-secretase inhibitor reduced neuropathic pain in the rat SNL model, whereas Jagged-1, a Notch ligand, increased pain sensitivity (Xie et al., 2015).

The failure of opioid antagonists to inhibit AAK1 inhibitor antinociception shows that AAK1 antinociception does not use the opioid system, a major inhibitory pain pathway used by endogenous and exogenous antinociceptives (Fields, 2004). Studies with α2 adrenergic agonists and opioids, however, raise the possibility that AAK1 inhibitors will synergize with opioids for antinociception. In particular, a major use

for clonidine, an α2 adrenergic agonist, is as an opioid adjuvant. Synergy of α2 adrenergic agonists and opioids is supported by preclinical (Stone et al., 2014) and clinical studies (Teasell et al., 2010; Engelman and Marsala, 2013). AAK1 inhibition may provide a means to obtain this synergy with the ease of oral delivery while avoiding the unwanted side effects of systemic α adrenergic agonism.

The structural diversity of these AAK1 inhibitors used in this study supports the conclusion from AAK1 knockouts that AAK1 inhibition is antinociceptive. It was difficult to identify AAK1 inhibitiors that did not inhibit BIKE. Relatively little is known about BIKE; however, it has been implicated in the differentiation of osteoclasts in vitro (Kearns et al., 2001). We found that BIKE knockouts were normal in the phenotyping battery, except for partial resistance to pain in the SNL model, and bred normally, and BIKE-AAK1 double knockouts were viable and healthy (data not shown).

We observed minor differences in the predicted plasma-free drug coverage of the cellular IC_{50} values in mice relative to rats. In particular, efficacious free plasma concentrations for LP-935509 averaged 30-fold and eightfold the cellular IC_{50} in mice and rats, respectively. These differences were most likely due to the sampling times to determine drug levels in which mice were typically sampled 30–120 minutes postdose, whereas rats were typically sampled 180–240 minutes postdose. Regardless of these differences, the comparison of free plasma drug levels with cellular IC_{50} values indicates that several fold coverage of the cellular IC_{50} is required for maximal antinociception.

The lack of significant nonpain-related phenotypes in the AAK1 knockout mice and AAK1 inhibitor–treated mice raises the hope that AAK1 inhibitors can provide antinociception without the side effects that limit current drugs targeting neuropathic pain. Gabapentinoids, such as gabapentin and pregabalin, which currently dominate the neuropathic pain market, are dose-limited by sedation and cognitive impairment and provide only very modest symptom control for most patients. We observe little or no separation between the minimum doses of gabapentin that produce efficacy in rat neuropathic pain models and those that cause impairment in the accelerating rotarod. Across the range of doses tested, those that produced significant efficacy also produced significant deficits in motor impairment. In contrast, in these same assays we have observed substantial separation between doses of AAK1 inhibitors that provide significant antinociceptive effect and the dose tested in motor impairment (which for AAK1 inhibitors failed to show any significant motor deficits at the maximum dose tested, suggesting potential for an even greater separation).

Using a large-scale mouse knockout and phenotypic screening approach, we identified AAK1 as a potential new target for neuropathic pain. We have further demonstrated that it is possible to generate brain-penetrant and orally active, selective AAK1 inhibitors with drug-like properties that are effective in both ligation and diabetic neuropathy models without dose-limiting side effects or alterations in normal nociception. We believe this represents a promising new direction for novel neuropathic pain therapy.

Acknowledgments

We thank Mian Gao, Yaqun Zhang, Brian Carpenter, Chunhong Yan, Frank Marsilo, John Newitt, and Nicholas Szapiel from Bristol-Myers Squibb (BMS) for expert production and purification of the recombinant kinases used in these studies; Kim Esposito and Ramesh Padmanabha of the BMS Lead Discovery and Optimization (LDO) Department for design and execution of the high throughput screen that produced the several important initial hits for the program; Shuli Wang of Lexicon for conducting a high throughput screen; Randi Brown of BMS LDO for expert execution of the AAK1 caliper assay; Jing Chen, Glen Farr, Michele Matchett, and Reshma Panemangalore of BMS LDO for receptor profiling in binding and functional assays; Krishna Pochá of BMS Biocon Research Center and Mike Donegan of BMS Preclinical Candidate Optimization (PCO) for analysis of biology and PK samples; and Ben Johnson of BMS PCO for skilled assessment of biotransformation. We acknowledge the chemistry efforts of SelvaKumar Bhaskaran, Tarun Maishal, Raju Manepalli, K.S. Maheswaran, Vivekananda Murthy Vrudhula, and Bireshwar Dasgupta.

Authorship Contributions

Participated in research design: Albright, Mandlekar, Vikramadithyan, Nara, Allen, Balakrishnan, Bristow, Brown, Carson, Denton, Dzierba, Bronson, Conway, Easton, Grace, Hamman, Kiss, Kostich, Lanthorn, Lentz, Li, Macor, Main, Nouraldeen, Santone, Savelieva, Baker, Swaffield, Westphal, Wilson, Ye, Zaczek, Zambrowicz.

Conducted experiments: Kumar, Das, Dokania, Shankar, Elavazhagan, Holenarsipur, Louis, Dandapani, Vattikundala, Sharma, Allen, Balakrishnan, Bi, Bourin, Brown, Feng, Grace, Gulianello, Hamman, Huang, Kiss, Lewis, Li, Lippy, Lu, Molski, Naidu, Nouraldeen, O'Malley, Pieschl, Savelieva, Baker, Ye.

Contributed new reagents or analytic tools: Hamman.

Performed data analysis: Allen, Balakrishnan, Bourin, Brown, Denton, Feng, Grace, Gulianello, Hamman, Kostich, Lentz, Li, Lippy, Nouraldeen, O'Malley, Savelieva, Baker, Swaffield, Westphal, Ye, Zambrowicz.

Wrote of contributed to the writing of the manuscript: Albright, Conway, Denton, Easton, Hamman, Kostich, Lentz, Li, Lippy, Savelieva, Baker, Zaczek, Zambrowicz.

References

Arendt-Nielsen L, Mansikka H, Staahl C, Rees H, Tan K, Smart TS, Monhemius R, Suzuki R, and Drewes AM (2011) A translational study of the effects of ketamine and pregabalin on temporal summation of experimental pain. *Reg Anesth Pain Med* **36**:585–591.

Beltran del Rio H, Kern F, Lanthorn T, Oravecz T, Piggott J, Powell D, Ramirez-Solis R, Sands AT, and Zambrowicz B (2003) Saturation screening of the druggable mammalian genome, in *Model Organisms in Drug Discovery* (Carroll P and Fitzgerald K eds) pp 251-278, Wiley & Sons, Chichester, UK.

Benarroch EE (2008) Descending monoaminergic pain modulation: bidirectional control and clinical relevance. *Neurology* **71**:217–221.

Bennett GJ and Xie YK (1988) A peripheral mononeuropathy in rat that produces disorders of pain sensation like those seen in man. *Pain* **33**:87–107.

Brommage R, Desai U, Revelli JP, Donoviel DB, Fontenot GK, Dacosta CM, Smith DD, Kirkpatrick LL, Coker KJ, and Donoviel MS, et al. (2008) High-throughput screening of mouse knockout lines identifies true lean and obese phenotypes. *Obesity* **16**:2362–2367.

Brommage R, Liu J, Hansen GM, Kirkpatrick LL, Potter DG, Sands AT, Zambrowicz B, Powell DR, and Vogel P (2014) High-throughput screening of mouse gene knockouts identifies established and novel skeletal phenotypes. *Bone Res* **2**:14034.

Chaplan SR, Bach FW, Pogrel JW, Chung JM, and Yaksh TL (1994) Quantitative assessment of tactile allodynia in the rat paw. *J Neurosci Methods* **53**:55–63.

Chaumont S, André C, Perrais D, Boué-Grabot E, Taly A, and Garret M (2013) Agonist-dependent endocytosis of γ-aminobutyric acid type A (GABAA) receptors revealed by a γ2(R43Q) epilepsy mutation. *J Biol Chem* **288**:28254–28265.

Conner SD and Schmid SL (2002) Identification of an adaptor-associated kinase, AAK1, as a regulator of clathrin-mediated endocytosis. *J Cell Biol* **156**:921–929.

Costigan M, Scholz J, and Woolf CJ (2009) Neuropathic pain: a maladaptive response of the nervous system to damage. *Annu Rev Neurosci* **32**:1–32.

Courteix C, Eschalier A, and Lavarenne J (1993) Streptozocin-induced diabetic rats: behavioural evidence for a model of chronic pain. *Pain* **53**:81–88.

D'Amour FE and Smith DL (1941) A method for determining loss of pain sensation. *J Pharmacol Exp Ther* **72**:74–79.

Dolphin AC (2012) Calcium channel auxiliary α2δ and β subunits: trafficking and one step beyond. *Nat Rev Neurosci* **13**:542–555.

Dubuisson D and Dennis SG (1977) The formalin test: a quantitative study of the analgesic effects of morphine, meperidine, and brain stem stimulation in rats and cats. *Pain* **4**:161–174.

Dunham NW and Miya TS (1957) A note on a simple apparatus for detecting neurological deficit in rats and mice. *J Am Pharm Assoc Am Pharm Assoc* **46**:208–209.

Engelman E and Marsala C (2013) Efficacy of adding clonidine to intrathecal morphine in acute postoperative pain: meta-analysis. *Br J Anaesth* **110**:21–27.

Fairbanks CA (2003) Spinal delivery of analgesics in experimental models of pain and analgesia. *Adv Drug Deliv Rev* **55**:1007–1041.
Fairbanks CA, Stone LS, and Wilcox GL (2009) Pharmacological profiles of alpha 2 adrenergic receptor agonists identified using genetically altered mice and isobolographic analysis. *Pharmacol Ther* **123**:224–238.
Fields H (2004) State-dependent opioid control of pain. *Nat Rev Neurosci* **5**:565–575.
Finnerup NB, Sindrup SH, and Jensen TS (2010) The evidence for pharmacological treatment of neuropathic pain. *Pain* **150**:573–581.
Gupta-Rossi N, Ortica S, Meas-Yedid V, Heuss S, Moretti J, Olivo-Marin JC, and Israël A (2011) The adaptor-associated kinase 1, AAK1, is a positive regulator of the Notch pathway. *J Biol Chem* **286**:18720–18730.
Hargreaves K, Dubner R, Brown F, Flores C, and Joris J (1988) A new and sensitive method for measuring thermal nociception in cutaneous hyperalgesia. *Pain* **32**:77–88.
Hayashida K, Obata H, Nakajima K, and Eisenach JC (2008) Gabapentin acts within the locus coeruleus to alleviate neuropathic pain. *Anesthesiology* **109**:1077–1084.
Hayashida K, Parker R, and Eisenach JC (2007) Oral gabapentin activates spinal cholinergic circuits to reduce hypersensitivity after peripheral nerve injury and interacts synergistically with oral donepezil. *Anesthesiology* **106**:1213–1219.
Hylden JL and Wilcox GL (1980) Intrathecal morphine in mice: a new technique. *Eur J Pharmacol* **67**:313–316.
Jackson AP, Flett A, Smythe C, Hufton L, Wettey FR, and Smythe E (2003) Clathrin promotes incorporation of cargo into coated pits by activation of the AP2 adaptor micro2 kinase. *J Cell Biol* **163**:231–236.
Kearns AE, Donohue MM, Sanyal B, and Demay MB (2001) Cloning and characterization of a novel protein kinase that impairs osteoblast differentiation in vitro. *J Biol Chem* **276**:42213–42218.
Kim SH and Chung JM (1992) An experimental model for peripheral neuropathy produced by segmental spinal nerve ligation in the rat. *Pain* **50**:355–363.
Kittler JT, Chen G, Kukhtina V, Vahedi-Faridi A, Gu Z, Tretter V, Smith KR, McAinsh K, Arancibia-Carcamo IL, and Saenger W, et al. (2008) Regulation of synaptic inhibition by phospho-dependent binding of the AP2 complex to a YECL motif in the GABAA receptor gamma2 subunit. *Proc Natl Acad Sci USA* **105**: 3616–3621.
Kuai L, Ong SE, Madison JM, Wang X, Duvall JR, Lewis TA, Luce CJ, Conner SD, Pearlman DA, and Wood JL, et al. (2011) AAK1 identified as an inhibitor of neuregulin-1/ErbB4-dependent neurotrophic factor signaling using integrative chemical genomics and proteomics. *Chem Biol* **18**:891–906.
Laird JM and Bennett GJ (1993) An electrophysiological study of dorsal horn neurons in the spinal cord of rats with an experimental peripheral neuropathy. *J Neurophysiol* **69**:2072–2085.
Liu C and Walker JM (2006) Effects of a cannabinoid agonist on spinal nociceptive neurons in a rodent model of neuropathic pain. *J Neurophysiol* **96**:2984–2994.
McCarson KE and Enna SJ (2014) GABA pharmacology: the search for analgesics. *Neurochem Res* **39**:1948–1963.
Mestre C, Pélissier T, Fialip J, Wilcox G, and Eschalier A (1994) A method to perform direct transcutaneous intrathecal injection in rats. *J Pharmacol Toxicol Methods* **32**:197–200.
Mogil JS (2009) Animal models of pain: progress and challenges. *Nat Rev Neurosci* **10**:283–294.
Montana MC, Conrardy BA, Cavallone LF, Kolber BJ, Rao LK, Greco SC, and Gereau RW, 4th (2011) Metabotropic glutamate receptor 5 antagonism with fenobam: examination of analgesic tolerance and side effect profile in mice. *Anesthesiology* **115**: 1239–1250.
Morrow TJ (2004) Animal models of painful diabetic neuropathy: the STZ rat model. *Curr Protoc Neurosci* Chapter 9:Unit 9.18.
Obata H, Saito S, Koizuka S, Nishikawa K, and Goto F (2005) The monoamine-mediated antiallodynic effects of intrathecally administered milnacipran, a serotonin noradrenaline reuptake inhibitor, in a rat model of neuropathic pain. *Anesth Analg* **100**:1406–1410, table of contents.
Powell DR, DaCosta CM, Gay J, Ding ZM, Smith M, Greer J, Doree D, Jeter-Jones S, Mseeh F, and Rodriguez LA, et al. (2013) Improved glycemic control in mice lacking Sglt1 and Sglt2. *Am J Physiol Endocrinol Metab* **304**:E117–E130.
Santos-Nogueira E, Redondo Castro E, Mancuso R, and Navarro X (2012) Randall-Selitto test: a new approach for the detection of neuropathic pain after spinal cord injury. *J Neurotrauma* **29**:898–904.
Shi B, Conner SD, and Liu J (2014) Dysfunction of endocytic kinase AAK1 in ALS. *Int J Mol Sci* **15**:22918–22932.
Snedecor SJ, Sudharshan L, Cappelleri JC, Sadosky A, Desai P, Jalundhwala Y, and Botteman M (2014) Systematic review and meta-analysis of pharmacological therapies for pain associated with postherpetic neuralgia and less common neuropathic conditions. *Int J Clin Pract* **68**:900–918.
Stone LS, German JP, Kitto KF, Fairbanks CA, and Wilcox GL (2014) Morphine and clonidine combination therapy improves therapeutic window in mice: synergy in antinociceptive but not in sedative or cardiovascular effects. *PLoS One* **9**: e109903.
Tang T, Li L, Tang J, Li Y, Lin WY, Martin F, Grant D, Solloway M, Parker L, and Ye W, et al. (2010) A mouse knockout library for secreted and transmembrane proteins. *Nat Biotechnol* **28**:749–755.
Tanimoto-Mori S, Nakazato-Imasato E, Toide K, and Kita Y (2008) Pharmacologic investigation of the mechanism underlying cold allodynia using a new cold plate procedure in rats with chronic constriction injuries. *Behav Pharmacol* **19**:85–90.
Teasell RW, Mehta S, Aubut JA, Foulon B, Wolfe DL, Hsieh JT, Townson AF, and Short C; Spinal Cord Injury Rehabilitation Evidence Research Team (2010) A systematic review of pharmacologic treatments of pain after spinal cord injury. *Arch Phys Med Rehabil* **91**:816–831.
Traub LM (2009) Tickets to ride: selecting cargo for clathrin-regulated internalization. *Nat Rev Mol Cell Biol* **10**:583–596.
Ultanir SK, Hertz NT, Li G, Ge WP, Burlingame AL, Pleasure SJ, Shokat KM, Jan LY, and Jan YN (2012) Chemical genetic identification of NDR1/2 kinase substrates AAK1 and Rabin8 uncovers their roles in dendrite arborization and spine development. *Neuron* **73**:1127–1142.
Wang G, Dai D, Chen X, Yuan L, Zhang A, Lu Y, and Zhang P (2014) Upregulation of neuregulin-1 reverses signs of neuropathic pain in rats. *Int J Clin Exp Pathol* **7**: 5916–5921.
Watzman N, Barry H, 3rd, Buckley JP, and Kinnard WJ, Jr (1964) Semiautomatic System for Timing Rotarod Performance. *J Pharm Sci* **53**:1429–1430.
Woolfe G and MacDonald AD (1944) The evaluation of the analgesic action of pethidine hydrochloride (Demerol). *J Pharmacol Exp Ther* **80**:300–307.
Xie K, Qiao F, Sun Y, Wang G, and Hou L (2015) Notch signaling activation is critical to the development of neuropathic pain. *BMC Anesthesiol* **15**:41.
Yaksh TL, Ozaki G, McCumber D, Rathbun M, Svensson C, Malkmus S, and Yaksh MC (2001) An automated flinch detecting system for use in the formalin nociceptive bioassay. *J Appl Physiol (1985)* 90:2386-2402.
Ye GL, Savelieva KV, Vogel P, Baker KB, Mason S, Lanthorn TH, and Rajan I (2015) Ligation of mouse L4 and L5 spinal nerves produces robust allodynia without major motor function deficit. *Behav Brain Res* **276**:99–110.
Zambrowicz BP and Sands AT (2003) Knockouts model the 100 best-selling drugs: will they model the next 100? *Nat Rev Drug Discov* **2**:38–51.
Zeilhofer HU, Ralvenius WT, and Acuña MA (2015) Restoring the spinal pain gate: GABA(A) receptors as targets for novel analgesics. *Adv Pharmacol* **73**: 71–96.

Address correspondence to: Dr. Charles F. Albright, Bristol-Myers Squibb, 5 Research Parkway, Wallingford, CT 06492. E-mail: Charlie.Albright@BMS.com or Dr. Brian Zambrowicz, Regeneron Pharmaceuticals, 777 Old Saw Mill River Road, Tarrytown, NY 10591. E-mail: brian.zambrowicz@regeneron.com

SUPPLEMENTAL MATERIALS AND METHODS

Inhibition of AAK1 kinase as a novel therapeutic approach to treat neuropathic pain

Walter Kostich[a], Brian D. Hamman[a], Yu-Wen Li, Sreenivasulu Naidu, Kumaran Dandapani, Jianlin Feng, Amy Easton, Clotilde Bourin, Kevin Baker, Jason Allen, Katerina Savelieva, Justin V. Louis, Manoj Dokania, Saravanan Elavazhagan, Pradeep Vattikundala, Vivek Sharma, Manish Lal Das, Ganesh Shankar, Anoop Kumar, Vinay K. Holenarsipur, Michael Gulianello, Ted Molski, Jeffrey M. Brown, Martin Lewis, Yanling Huang, Yifeng Lu, Rick Pieschl, Kevin O'Malley, Jonathan Lippy, Amr Nouraldeen, Thomas H. Lanthorn, Guilan Ye, Alan Wilson, Anand Balakrishnan, Rex Denton, James E. Grace, Kimberley A. Lentz, Kenneth S. Santone, Yingzhi Bi, Alan Main, Jon Swaffield, Ken Carson, Sandhya Mandlekar, Reeba K. Vikramadithyan, Susheel J. Nara, Carolyn Dzierba, Joanne Bronson, John E. Macor, Robert Zaczek, Ryan Westphal, Laszlo Kiss, Linda Bristow, Charles M. Conway, Brian Zambrowicz[b], and Charles F. Albright[b]

Journal of Pharmacology and Experimental Therapeutics

Synthesis of AAK1 inhibitors

All reactions were carried out under a nitrogen atmosphere with anhydrous, commercial grade solvents, unless otherwise noted. All other reagents and solvents were reagent grade and used as received from commercial sources. Nuclear magnetic resonance (NMR) chemical shifts (δ) are reported in parts per million relative to internal tetramethylsilane (TMS). Yields refer to chromatographically and spectroscopically homogeneous materials, unless otherwise stated.

Synthesis of 4-[3-(2-Methoxy-pyridin-3-yl)-pyrazolo[1,5-*a*]pyrimidin-5-yl]-piperazine-1-carboxylic acid isopropyl ester (LP-935509) (Bi et al., 2015b)

Part A: **3-Bromo-5-piperazin-1-ylpyrazolo[1,5-*a*]pyrimidine**

3-Bromo-5-chloro-pyrazolo[1,5-a]pyrimidine (15.4 g, 66.2 mmol) and piperazine (56.8 g, 659.5 mmol) were ground together in a mortar to an intimate mixture and transferred to a 250 mL round-bottomed flask containing a magnetic stir bar. The flask was fitted to a reflux condenser, N_2 blanketed, and the reaction pot immersed in an ambient temperature oil bath. While the neat solid mixture stirred, the bath was heated to 120 ^oC over 0.5 h and held at that temperature for a total of 2 h. The bath was removed and the molten reaction allowed to cool to approximately 75 ^oC. Ethyl acetate was cautiously added down the condenser to dissolve the reaction product to prevent its setting up into a solid mass. The reaction solution was transferred to a separatory funnel, further diluted with ethyl acetate, and washed with water. The ethyl acetate extract was dried ($MgSO_4$) and evaporated to obtain 16.1 g of clear yellow oil. The oil was crystallized from methanol to provide 15.8 g of light yellow crystalline powder of 3-bromo-5-piperazin-1-ylpyrazolo[1,5-*a*]pyrimidine in two crops, mp. 108-109 ^oC. ^1H NMR (400 MHz, dimethylsulfoxide (DMSO)-d_6) δ ppm 2.51 (s, 1 H) 3.16 - 3.24 (m, 3 H) 3.38 (s, 1 H) 3.93 - 4.00 (m, 3 H) 6.85 (d, *J*=7.83 Hz, 1 H) 8.03 (s, 1 H) 8.78 (d, *J*=8.08 Hz, 1 H) 9.61 (br. s., 1 H). ^{13}C NMR (100 MHz, DMSO-d_6) δ ppm 41.25, 42.16, 77.73, 97.78, 136.77, 144.01, 144.18, 155.53. LRMS (ESI) *m/z* 282.0/284.0 $[(M+H)]^+$, calc'd for $C_{10}H_{12}BrN_5$: 282.14.

Part B: **4-(3-Bromopyrazolo[1,5-a]pyrimidin-5-yl)piperazine-1-carboxylic acid isopropyl ester**

To a rapidly stirred, 0 ^oC, N_2 blanketed, solution of 3-bromo-5-piperazin-1-yl-pyrazolo[1,5-*a*]pyrimidine (15.8 g, 56.0 mmol) and Hunig's base (20.0 mL, 114.8 mmol) in ethyl acetate (280 mL) was steadily added a 1.0 M solution of isopropyl chloroformate in toluene (67.0 mL) over the course of 10 min. The reaction was allowed to stir and warm to ambient temperature over night at which time it was washed with brine, dried ($MgSO_4$), preloaded onto silica gel, chromatographed (Silica gel, eluted with 100% ethyl

acetate) and crystallized from ethyl acetate / heptane to afford 13.2 g of the titled compound as white powder, mp. 78-79 °C. ^{1}H NMR (400 MHz, DMSO-d_6) δ ppm 1.22 (d, *J*=6.32 Hz, 6 H) 3.44 - 3.54 (m, 4 H) 3.67 - 3.79 (m, 4 H) 4.82 (spt, *J*=6.23 Hz, 1 H) 6.77 (d, *J*=7.83 Hz, 1 H) 7.97 (s, 1 H) 8.69 (d, *J*=7.83 Hz, 1 H). ^{13}C NMR (100 MHz, DMSO-d_6) δ ppm 21.94, 42.80, 43.87, 68.17, 77.32, 97.66, 136.47, 143.87, 144.40, 154.29, 155.64. LRMS (ESI) *m/z* 368.0/370.0 $[(M+H)]^+$, calc'd for $C_{14}H_{18}BrN_5O_2$: 368.24.

Part C: **4-[3-(2-Methoxy-pyridin-3-yl)pyrazolo[1,5-*a*]pyrimidin-5-yl]-piperazine-1-carboxylic acid isopropyl ester**

To a mixture of 4-(3-bromo-pyrazolo[1,5-*a*]pyrimidin-5-yl)-piperazine-1-carboxylic acid isopropyl ester (338.7 mg, 0.9 mmol), 2-methoxy-3-pyridineboronic acid (169.4 mg, 1.1 mmol), potassium phosphate tribasic monohydrate (423.9 mg, 1.84 mmol), and [1,1′-bis(diphenylphosphino)ferrocene]dichloropalladium(II), complex with dichloromethane (78.6 mg, 0.1 mmol) contained in a 50 mL round-bottomed flask was added a solution of 30% (v/v) water in 1,2-dimethoxyethane (17 mL) and a magnetic stir bar. The reaction pot was fitted to a reflux condenser, lowered into an ambient temperature oil bath, and the system taken through 10 evacuation / N_2 blanket cycles while being rapidly stirred. The rapidly stirred, N_2 blanketed, reaction was heated to an oil bath temperature of 85 °C for 17 h then cooled and partitioned between brine (pH adjusted to 10 with 3N aqueous sodium hydroxide) and ethyl acetate. The separated organic layer was dried ($MgSO_4$) and evaporated to afford an oil which was purified by preparative reverse phase-HPLC to afford 76.0 mg of the titled compound as a free base. ^{1}H NMR (400 MHz, DMSO-d_6) δ ppm 1.22 (d, *J*=6.06 Hz, 6 H) 3.47 - 3.56 (m, 4 H) 3.71 - 3.80 (m, 4 H) 4.00 (s, 3 H) 4.82 (spt, *J*=6.23 Hz, 1 H) 6.81 (d, *J*=8.08 Hz, 1 H) 7.08 (dd, *J*=7.45, 4.93 Hz, 1 H) 7.98 (dd, *J*=4.93, 1.89 Hz, 1 H) 8.51 (s, 1 H) 8.76 (d, *J*=7.83 Hz, 1 H) 8.82 (dd, *J*=7.58, 2.02 Hz, 1 H). ^{13}C NMR (100 MHz, DMSO-d_6) δ ppm 21.95, 42.85, 44.06, 53.10, 68.16, 97.21, 98.90, 116.40, 117.17, 134.55, 136.43, 141.99, 144.65, 144.71, 154.26, 155.46, 158.89. LRMS (ESI) *m/z* 397.1 $[(M+H)]^+$, calc'd for $C_{20}H_{24}N_6O_3$: 396.45.

Synthesis of (2-[3-(4-Carbamoyl-phenyl)imidazo[1,2-*b*]pyridazin-6-ylamino]ethyl)methylcarbamic acid tert-butyl ester (LP-922761) (Bi et al., 2015a)

Part A: **6-fluoroimidazo[1,2-*b*]pyridazine**

6-Fluoropyridazin-3-ylamine (10 g, 89 mmol) was combined with a 50% (w/v) aqueous solution of chloroacetaldehyde (23 mL, 177 mmol) in *n*-butanol (150 mL) and stirred at reflux for 1h. The cooled reaction solution was reduced in volume and diluted with diethyl ether to precipitate a brown solid, which was collected by filtration, to yield 12.0 g of the titled compound. LRMS (ESI) *m/z* 138.0$[(M+H)]^+$, calc'd for $C_6H_4FN_3$: 137.12.

Part B: **3-bromo-6-fluoroimidazo[1,2-*b*]pyridazine**

To an ambient temperature, stirred solution of 6-fluoroimidazo[1,2-*b*]pyridazine (2.1 g, 15.3 mmol) in glacial acetic acid (20 mL) was slowly added bromine (2.5 g, 15.3 mmol). Upon completion of this addition, the reaction solution was poured into water and extracted with ethyl acetate. The extract was dried ($MgSO_4$) and flash chromatographed (silica gel, eluted with 30% (v/v) ethyl acetate / hexanes) to provide 0.9 g of 3-bromo-6-fluoro-imidazo[1,2-*b*]pyridazine. LRMS (ESI) *m/z* 215.9/217.9 $[(M+H)]^+$, calc'd for $C_6H_3BrFN_3$: 216.01.

Part C: **[2-(3-Bromoimidazo[1,2-*b*]pyridazin-6-ylamino)ethyl]methylcarbamic acid tert-butyl ester**

A solution of 3-bromo-6-fluoroimidazo[1,2-*b*]pyridazine (1.4 g, 6.3 mmol), *N*-(2-aminoethyl)-n-methyl carbamic acid *tert*-butyl ester (961 mg, 5.5 mmol), and Hunig's base (1.1 mL, 6.4 mmol) in 2-propanol (28 mL) was heated to reflux for 4 d, cooled, preloaded onto silica gel and flash chromatographed (silica gel eluted with 10% (v/v) methanol /ethyl acetate). The isolated light yellow solid product was recrystallized (ethyl acetate/heptane) to yield 1.2 g of [2-(3-bromoimidazo[1,2-*b*]pyridazin-6-ylamino)ethyl]methylcarbamic acid *tert*-butyl ester as a white powder, mp. 128-129 ^oC. ^1H NMR (400 MHz, DMSO-d_6) δ ppm (rotamers present) 1.16 (s, 6 H) 1.33 (br. s., 3 H) 2.84 (s, 2 H) 2.90 (br. s., 1 H)

3.34 - 3.44 (m, 3 H) 3.45 - 3.52 (m, 1 H) 6.68 (d, *J*=9.60 Hz, 1 H) 7.31 (br. s., 1 H) 7.49 (s, 1 H) 7.72 (d, *J*=9.35 Hz, 1 H). ^{13}C NMR (100 MHz, DMSO-d_6) δ ppm 28.22, 28.45, 34.02, 35.07, 39.02, 39.97, 46.23, 47.06, 78.52, 78.87, 99.57, 113.35, 125.92, 130.80, 137.01, 154.37, 155.39. LRMS (ESI) *m/z* 370.1/372.1 $[(M+H)]^+$, calc'd for $C_{14}H_{20}BrN_5O_2$: 370.25.

Part D: **(2-[3-(4-Carbamoylphenyl)imidazo[1,2-*b*]pyridazin-6-ylamino]ethyl)methylcarbamic acid tert-butyl ester**

To a mixture of [2-(3-bromoimidazo[1,2-*b*]pyridazin-6-ylamino)ethyl]methylcarbamic acid *tert*-butyl ester (367.4 mg, 1.0 mmol), (4-carbamoylphenyl)boronic acid (196.7 mg, 1.2 mmol), potassium phosphate tribasic monohydrate (418.4 mg, 1.8 mmol), and [1,1′-bis(diphenylphosphino)ferrocene]dichloropalladium(II), complex with dichloromethane (82.1 mg, 0.1 mmol) in a round-bottomed flask was added a solution of 30% (v/v) water in 1,2-dimethoxyethane (25 mL) and a magnetic stir bar. The reaction pot was fitted to a reflux condenser, lowered into an ambient temperature oil bath, and the system taken through 10 evacuation / N_2 blanket cycles while being rapidly stirred. The rapidly stirred, N_2 blanketed, reaction was heated to an oil bath temperature of 85 ^oC for 17 h then cooled and partitioned between brine and ethyl acetate. The separated organic layer was dried ($MgSO_4$), evaporated, flash chromatographed (silica gel eluted with 100% ethyl acetate) and crystallized (ethyl acetate/heptane) to provide 2-([3-(4-carbamoylphenyl)imidazo[1,2-*b*]pyridazin-6-ylamino]ethyl)methylcarbamic acid *tert*-butyl ester (135.6 mg) as white powder, mp. 190-191 ^oC (dec.). ^{1}H NMR (400 MHz, DMSO-d_6) δ ppm (rotamers present) 1.15 (br. s., 5 H) 1.28 (br. s., 1 H) 1.38 (br. s., 3 H) 2.85 (br. s., 3 H) 3.32 (br. s., 1 H) 3.54 (br. s., 1 H) 6.73 (d, *J*=9.35 Hz, 1 H) 7.27 (br. s., 1 H) 7.34 (br. s., 1 H) 7.79 (d, *J*=9.60 Hz, 1 H) 7.94 - 8.03 (m, 4 H) 8.28 (d, *J*=8.08 Hz, 2 H). LRMS (ESI) *m/z* 411.2 $[(M+H)]^+$, calc'd for $C_{21}H_{26}N_6O_3$: 410.48.

Synthesis of (*S*)-8-((2-amino-4-methylpentyl)oxy)-4,6-dimethyl-5-oxo-5,6-dihydrobenzo[*c*][2,7]naphthyridine-9-carbonitrile(BMS-090605)

Compound BMT-090605 was prepared as described in WO Patent #022,167 (2014), Example 64 (Vrudhula et al., 2014).

Synthesis of (*S*)-*N*-(8-((2-amino-2,4-dimethylpentyl)oxy)-5*H*-chromeno[3,4-*c*]pyridin-2-yl)acetamide (BMS-124110)

Compound BMT-124110 was prepared as described in WO Patent #038,112 (2015), Example 45 (Vrudhula et al., 2015).

Synthesis of 3-((5-((4-aminopiperidin-1-yl)methyl)pyrrolo[2,1-*f*][1,2,4]triazin-4-yl)amino)-5-(2-isopropyl-2*H*-tetrazol-5-yl)phenol (BMS-901715)

Compound BMS-901715 was prepared as described in patent WO 2015/054358 A1 Example 36.

Synthesis of [3H]-*Tert*-butyl (*S*)-2-(((3-(2-methoxyphenyl)pyrazolo[1,5-*a*]pyrimidin-5-yl)amino)methyl)pyrrolidine-1-carboxylate (LP-927443)

LP-927443 was prepared in a manner similar as described in patent WO 2013/134228 A1 Example 5. 6. 12.

[3H]-*Tert*-butyl (*S*)-2-(((3-(2-methoxyphenyl)pyrazolo[1,5-*a*]pyrimidin-5-yl)amino)methyl)pyrrolidine-1-carboxylate was prepared as described in patent application WO 2013/134228 A1, Example 5.12.9 using 2-(4,4,5,5-tetramethyl-1,3,2-dioxaborolan-2-yl)phenol as the coupling partner to obtain *tert*-butyl (*S*)-2-(((3-(2-hydroxyphenyl)pyrazolo[1,5-*a*]pyrimidin-5-yl)amino)methyl)pyrrolidine-1-carboxylate. To *tert*-butyl (*S*)-2-(((3-(2-hydroxyphenyl)pyrazolo[1,5-*a*]pyrimidin-5-yl)amino)methyl)pyrrolidine-1-carboxylate (2.0 mg, 4.88 mmol) and Cs_2CO_3 (2.3 mg, mmol) in DMF (0.5 ml) was added [H-3]MeI (100 mCi). The reaction was stirred at ambient temperature for 1.5 hrs. HPLC analysis showed one major peak corresponding to the product. The crude sample was purified by

reverse phase HPLC (Luna 5u C18(2) (4.6X150); B: 1% TEAA (pH~4); D: CH_3CN; 1.2 mL/min; 265 nm; 0-20 min 50%D; 20-25 min 50-100%D; 25-30 min 100%D) to obtain[3H]-*tert*-butyl (*S*)-2-(((3-(2-methoxyphenyl)pyrazolo[1,5-*a*]pyrimidin-5-yl)amino)methyl)pyrrolidine-1-carboxylate. Product retention time: 16.23 min; S.A.=83.1 Ci/mmol, Radiochemical purity=99.9%, 2mCi/mL in 90% EtOH, 16.5 mL, 33 mCi.

Baculovirus expression of recombinant protein kinases

Recombinant baculovirus encoding protein kinase domains were constructed using the Bac-to-Bac system from Invitrogen™ (ThermoFisher Scientific) and were used to infect suspension cultures of insect cells and express the recombinant proteins essentially as described previously (Kiefer *et al.*, 2014). The AAK1 (NCBI RefSeq accession NP_055726.3) kinase domain was expressed using a recombinant baculovirus vector encoding amino acids 9-330 fused behind glutathione S-transferase and an intervening Factor Xa cleavage site to produce GST-Xa-hAAK1(29-330). The amplified P2 virus was used to infect High Five™ (ThermoFisher Scientific) insect cells in suspension culture at 10.5 liter scale. The cells were harvested by sedimentation 62 h post-infection and yielded 329 grams of cell paste that was frozen at -80°C. Similarly, the GAK (NCBI RefSeq accession NP_005246.2) kinase domain was expressed using recombinant baculovirus encoding GST-Xa-hGAK(12-347). The infected cells from 3.5 liters of suspension culture were harvested by sedimentation 65 h post-infection and yielded 68 grams of cell paste that was frozen. The kinase domain of BMP2K (NCBI RefSeq accession NP_942595.1) was expressed using recombinant baculovirus encoding GST-Xa-hBMP2K(1-367). The infected cells from 10 liters of suspension culture were harvested by sedimentation 52 h post-infection and yielded 120 grams of cell paste that was frozen.

Purification of recombinant protein kinases

Pellets of frozen cell paste (113 grams) from the GST-Xa-hAAK1(29-330) expression were thawed by stirring in 350 ml Lysis Buffer (PBS pH 7.4 supplemented with 2 mM EDTA, 0.5% w/v Triton X-100, 1

mM DTT, 4 tablets SigmaFAST™ protease inhibitor, 25 U/ml Benzonase® nuclease). All subsequent steps were performed on ice or at 4 °C. The cell suspension was lysed by sonication with a Branson Sonifier equipped with a flat tip probe operated at 70% power with 4 x 40 second intervals (interval duty cycle 2 sec ON, 0.3 sec OFF) with swirling on ice between intervals to prevent warming. The lysate was clarified by sedimentation for 40 minutes at 15,000 x g. The clarified lysate was mixed with 10 ml packed Glutathione Sepharose 4 Fast Flow medium (GE Healthcare Life Sciences) that had been pre-washed with Lysis Buffer, and the suspension was mixed gently by rocking for 90 minutes. The medium was collected by sedimentation and transferred to a XK16/20 column (GE Healthcare Life Sciences), and the lysate was applied and allowed to flow through the packed medium. The column was washed with 100 ml of Wash Buffer (PBS, pH 7.4 supplemented with 2 mM EDTA and 1 mM DTT), and then eluted with 100 ml of Wash Buffer plus 20 mM reduced glutathione into 5 ml fractions. The protein content of the eluted fractions was analyzed by SDS-PAGE and Coomassie Brilliant Blue staining, and fractions enriched in GST-Xa-hAAK1(29-330) were pooled. The pool was concentrated 8-fold by centrifugal ultrafiltration with Amicon Ultra-15 units with 30-kDa cutoff (EMD Millipore) and then loaded onto a HiLoad 26/600 Superdex 200 pg size exclusion chromatography (SEC) column (GE Healthcare Life Sciences) equilibrated with PBS pH 7.4 containing 2 mM EDTA, 1 mM DTT, and 10% v/v glycerol. The fractions containing the intact GST-Xa-hAAK1(29-330) fusion protein were pooled, and the protein was concentrated by centrifugal ultrafiltration to 1.3 mg/ml, analyzed, divided into aliquots, flash frozen in liquid nitrogen, and stored at -80 °C. The final protein (yield 9.1 mg) appeared to be a discrete dimer by dynamic light scattering analysis (r_H = 4.7 nm) and had a mass of 60,324 Da by electrospray ionization mass spectrometry, consistent with the intact, *des*-Met protein.

The GST-Xa-hGAK(12-347) was purified with a glutathione-affinity plus Superdex 200SEC method similar to that used for the hAAK1 construct except that it was further purified by diluting the SEC protein pool 1:5 with 20 mM Tris-HCl pH 7.4, 10 mM NaCl and then loading onto a Q-Sepharose Fast Flow (GE Healthcare Life Sciences) column (2.6 x 11 cm). The protein was eluted with a NaCl gradient,

and fractions enriched in GST-Xa-hGAK(12-347) were pooled in a final buffer of 19 mM Tris, pH 7,4, 200 mM NaCl, 5 mM DTT, 5% glycerol, concentrated to 2.66 mg/ml by centrifugal ultrafiltration, divided into aliquots, flash frozen in liquid nitrogen, and stored at -80 °C. The final protein (yield 223 mg from 33 grams cell paste) appeared to be approximately a dimer by dynamic light scattering analysis (r_H = 5.7 nm) an mass by electrospray ionization mass spectrometry consistent with intact, *des*-Met GST-Xa-hGAK(12-347).

The GST-Xa-hBMP2K(1-367) was purified with a glutathione-affinity plus Superdex 200SEC method similar to that used for the hAAK1 construct except that the cells were lysed by nitrogen cavitation instead of sonication. The cells (40 grams) were suspended in 160 ml buffer containing PBS pH 7.4 supplemented with 200 mM NaCl, 5 mM $MgCl_2$, 5% glycerol, 25 U/ml Benzonase, 2 tablets Complete™ EDTA-minus protease inhibitor tablets (Roche Diagnostics) and lysed by nitrogen cavitation using a Nitrogen Bomb apparatus (#4635, Parr Instrument Company) pressurized to 300 psi for 30 minutes at 4°C. The lysate produced after depressurization was clarified by sedimentation at 100,000 x g for 30 minutes, and the supernatant was purified using 15 ml of Glutathione Sepharose 4 Fast Flow medium (GE Healthcare Life Sciences). The final protein from the size exclusion column (45 mg) was 1.3 mg/ml in a buffer of PBS, 5% (v/v) glycerol, 2 mM DTT, appeared to be approximately a dimer by dynamic light scattering analysis (r_H = 5.9 nm), and had a mass by electrospray ionization mass spectrometry consistent with intact, *des*-Met GST-Xa-hBMP2K(1-367). The final protein was divided into aliquots, flash frozen in liquid nitrogen, and stored at -80 °C.

AAK1 Kinase Assay – IC_{50} determination

Recombinant GST-Xa-hAAK1 (amino acids 30-330) was combined with a fluorescent substrate (5-FAM)-Aha-KEEQSQITSQVTGQIGWR-NH2) (CPC Scientific), ATP, and varying concentrations of inhibitors in a 384 well plate (Thermo Scientific). The final reaction volume (0.030 ml) contained 10 mM Tris-HCL pH 7.4, 10 mM $MgCl_2$, 0.01% Tween-20, 1.0 mM DTT, 22 µM ATP, 1.5 µM (5-FAM)-Aha-

KEEQSQITSQVTGQIGWR-NH2, 3.5 nM GST-Xa-hAAK1, 1.6% DMSO, and varying concentrations of inhibitors (from 2 μM to 33 pM). Compound stock solutions (10 mM) were prepared in DMSO. Kinase reactions were incubated at room temperature for 3 h and terminated by adding 60 μl of 35 mM EDTA buffer to each sample. Reaction solutions were analyzed on the Caliper LabChip 3000 (Caliper, Hopkinton, MA) by electrophoretic separation of the fluorescent substrate and phosphorylated product. IC_{50} values were derived by non-linear regression analysis of the concentration response data. The experimentally determined AAK1 ATP Km value was 22 μM.

AAK1 Kinase Assay – Compound kinetic study

Recombinant GST-Xa-hAAK1 (30-300) (PS) was combined with a fluorescent substrate FITC-AHA-KEEQSQITSQVTGQIGWR, ATP, and varying concentrations of inhibitors in a 384 well plate (Thermo Scientific). The final reaction volume (30 μl) contained 20 mM HEPES pH 7.4, 10 mM MgCl2, 0.015% Brij-35, 0.01 mg/ml BSA, 1 mM DTT, 1.5 mM FITC-{Aha}KEEQSQITSQVTGQIGWR, 5 nM GST-Xa-hAAK1, 1.6% DMSO, and varying concentrations of ATP (from 1 mM to 8 μM) and LP-935509 (from 250 nM to 13 pM). Compound stock solutions (10 mM) were prepared in DMSO. Kinase reactions were analyzed in real time at room temperature for 3 h on the Caliper LabChip 3000 (Perkin Elmer, Waltham, MA) by electrophoretic separation of the fluorescent substrate and phosphorylated product. Resultant data was plotted and globally fit to a competitive inhibition model using Graphpad Prism software version 5.01 (Graphpad, San Diego, CA).

BIKE Kinase Assay

Recombinant GST-BIKE was combined with a fluorescent substrate FITC-{Aha}KEEQSQITSQVTGQIGWR (P13BMS Peptide), ATP, and varying concentrations of inhibitors in a 384 well plate (Thermo Scientific). The final reaction volume (0.030 ml) contained 10 mM Tris-HCL pH 7.4, 10 mM $MgCl_2$, 0.01% Tween-20, 1.0 mM DTT, 3.3 μM ATP, 1.5 mM FITC-{Aha}KEEQSQITSQVTGQIGWR, 20 nM GST-BIKE, 1.6% DMSO, and varying concentrations of

inhibitors (from 2 μM to 33 pM). Compound stock solutions (10 mM) were prepared in DMSO. Kinase reactions were incubated at room temperature for 3 h and terminated by adding 60 ml of 35 mM EDTA buffer to each sample. Reaction solutions were analyzed on the Caliper LabChip 3000 (Caliper, Hopkinton, MA) by electrophoretic separation of the fluorescent substrate and phosphorylated product. IC_{50} values were derived by non-linear regression analysis of the concentration response data. The experimentally determined BIKE ATP Km value was 3.3 μM.

GAK radiometric kinase assay

Enzymatic activity of GAK was determined by phosphorylated product detection in a ^{33}P filter-binding assay using histone H1 protein (Millipore) as substrate. The assay mixture contained 100 nM recombinant GST-Xa-GAK (12-347) and 2 μM histone in a buffer containing 50 mM Tris, pH 7.5 containing 10 mM $MgCl_2$, 2 mM DTT, and 0.5 mM EGTA. Compound stock solutions (10 mM) were prepared in DMSO and varying concentrations (from 100 μM to 1.7 nM) were added to the plate via ECHO acoustic transfer (Labcyte, Sunnyvale, CA). Reaction was initiated with the addition of 40 μM ATP (final) and [γ-^{33}P]-ATP to a final volume of 30 μl and quenched after 60 minutes with 30 μl 300 mM phosphoric acid. Sample was transferred to the phosphocellulose membrane filtration plate using a Biomek FX liquid handling station (Beckman Coulter), where it was subsequently aspirated and washed five times with 75 mM phosphoric acid. The plate was dried in a 65 °C oven for 10 minutes, the bottom was sealed and 20 μl Microscint-20 was added to the plate. The plate was then read on a Topcount plate reader (Perkin Elmer, Waltham, MA). The experimentally determined GAK ATP Km value was 52 μM.

AMBIT /DiscoveRx Kinome Scan

Dry test compounds were provided to AMBIT/DiscoveRx for evaluation in their KINOMEscan panel. Compounds were resuspended and diluted in DMSO prior to inclusion in the assay at a final concentration of 1 μM. The ability of test compound to compete with proprietary ATP binding site probes

was evaluated for 389 kinases (Davis et al., 2011). Inhibition of probe binding was expressed as % control binding.

AAK1 radioligand binding assay

C57Bl6 mouse brains were homogenized in ice cold hypotonic lysis buffer (10 mM Tris buffer pH7.4 with 5 mM EDTA and 1 µl/ml Sigma protease inhibitor cocktail) using a polytron. The homogenate was centrifuged at 32000xg for 20 minutes and the resulting pullet was resuspended in homogenate wash buffer (50 mM Tris buffer pH 7.4 with 5 mM EDTA and 1 µl/ml Sigma protease inhibitor) and centrifuged again at 32000xg for 20 minutes. The resulting pellets were resuspended in assay buffer (120 mM NaCl, 5 mM KCl, 2 mM $CaCl_2$, 2 mM $MgCl_2$, and 50 mM Tris buffer (pH 7.4)) and frozen in aliquots at a protein concentration of 2.5 mg/ml and stored at -70 °C until use. Test compounds were evaluated for their ability to displace the AAK1 ATP binding site inhibitor 3H-LP-927443 (AAK1 Kd=467±56 pM (data not shown), specific activity 83.1 Ci/mmol) from mouse brain membrane homogenates. Non-specific binding was defined using an AAK1 inhibitor from a different chemotype BMS-901715 (AAK1 IC_{50}=200 pM). Competition binding assays were carried out in 96 well plates at room temperature. All reagents were prepared in assay buffer. The radioligand was diluted in assay buffer containing 1% BSA. Briefly 2 µl of test compound (11 point dose response curves) or non specific inhibitor control (final concentration 1 µM) were added to the plate, followed by 20 µl of ^{3}H-LP-927443 (final concentration 0.5 nM) and 180 µl of mouse brain homogenate (final concentration 8 µg/ml). Plates were vortexed to ensure complete mixing. During the 1 h incubation the plates were vortexed again at 30 minutes and 60 minutes. The assay was terminated by filtration through GF/B filters (presoaked in 0.5% polyethyleneimine) using a Brandel Harvestor. Filters were washed three times with ice cold wash buffer (assay buffer with 0.1% BSA). The filter circles were punched into a plate, Perkin Elmer Optiphase Supermix scintillation fluid was added and the plate was read using a Wallac 1450 Microbeta Trilux Liquid Scintillation Counter. IC_{50} values were derived by non-linear regression analysis of the concentration response data.

AAK1 Cellular Assay

HEK293F cells were cultured in media containing DMEM (Gibco, cat. #11965), 10% FBS (SAFC Biosciences, cat. #12103C), 1X GPS (glutamine, penicillin and streptomycin). On day one, 12 million cells were plated on a 10 cm dish at ~80% confluent. On day two, each 10 cm dish was transfected with 48 µg DNA (3 µg AAK1/HA/pIRES (full length human, NCBI accession no. NP_055726.2), 45 µg Flag/AP2MI/pcDNA (full length human, NCBI accession no. NM_004068.3), 144 µl Lipofectamine 2000 (Invitrogen, cat.# 11668-019), and 1.5 ml OPTI-MEM per manufacturer's instructions. On day three, cells were resuspended, pelleted by centrifugation at 1000 rpm for 5 min, and resuspended in 2.75 ml DMEM + 0.5% FBS. An aliquot of cells (100 µl) was transferred to each well in a 96 well plate. Compounds were dissolved in DMSO and diluted in DMSO to 1000 times the final concentration. Compound solutions (1 µl) were then mixed in 500 µl DMEM + 0.5% FBS and 100 µl of diluted compound were added to each well. Plates were then incubated at 37 °C and 5% CO_2 for 3 h. Cells were then resuspended and pelleted in a tube. For Western Blot analysis, cell pellets were resuspend in 40 µl 1X LDS-PAGE sample buffer (Invitrogen, cat.# NP0008) + 2X Halt phosphatase and protease inhibitor cocktail (Thermo Scientific, cat.#1861284), followed by sonication with microtip sonicator set at 5 for 8-10 seconds. Five µl of 10X NuPage Sample Reducing Agent (with 50 mM DTT) was to each sample followed by heat denaturing at 70 °C for 10 min. Each sample (10 µl) was loaded on a 4-20% Tris-Glycine Criterion 26-well gel (Biorad, cat.# 345-0034) for the phospho-µ2 blot and 10 µl per lane in a 4-12% Bis-Tris (+MES buffer) NuPAGE 26-well gel (Invitrogen, cat.# WG1403BX10) for the µ2 blot. For controls, 2 ng of phospho-µ2 or 20 ng µ2/Flag proteins were loaded on each gel. After SDS-PAGE, samples were transferred to PVDF membrane and membranes were blocked for one hour in TBST + 5% milk, followed by wash 3X for 5-10 min with TBST. Membranes were probed with rabbit anti-phospho-µ2 (1:5000; a rabbit polyclonal antibody produced by New England Peptide and affinity purified at Lexicon) in TBST + 5% BSA. NuPAGE gels were probed with mouse anti-Flag (1:500; Sigma, cat.# F1804) in TBST + 5% milk, and these primary antibodies were incubated overnight at 4 °C on a rocker.

On day four, Western blots were washed 3X for 5-10 minutes with TBST, probe with anti-rabbit-HRP (1:2000; BioRad, cat.# 170-6515) or anti-mouse-HRP (1:2000; Biorad, cat.# 170-6516) in TBST + 5% milk for 1 hour at RT, washed 3X for 10 minutes with TBST, and developed with ECL reagent (GE Healthcare, cat.# RPN2132) on a Versadoc. Images were captured with a camera and percent inhibition was calculated for each sample by first normalizing to total μ2 expression levels and then comparing to 0% and 100% controls. IC_{50} values were then calculated using Excel fitting software.

SUPPLEMENTAL REFERENCES

Bi Y, Gardyan MW, Green MA, Godwin K and Zhang Y (2015a) Imidazo[1,2-b]pyridazine-based compounds, and compositions, for treatment, management or prevention of disorders mediated by adaptor assocd. kinase 1, in.

Bi Y, W. M, Green MA, Godwin K and Zhang Y (2015b) Pyrazolo[1,5-a]pyrimidine-based compounds, compositions comprising them, and methods of use, in.

Davis MI, Hunt JP, Herrgard S, Ciceri P, Wodicka LM, Pallares G, Hocker M, Treiber DK and Zarrinkar PP (2011) Comprehensive analysis of kinase inhibitor selectivity. *Nature biotechnology* **29**:1046-1051.

Vrudhula VM, Pan S, Rajamani R, Macor JE, Bronson JJ, Dzierba CD, Nara SJ and Karatholuvhu MS (2015) Preparation of chromenopyridine derivatives for use as adaptor associated kinase 1 inhibitors, in.

Vrudhula VM, Pan S, Rajamani R, Nara SJ, Karatholuvhu MS, Maishal TK, Ditta JL, Dzierba CD, Bronson JJ and Macor JE (2014) Preparation of aryl lactam kinase inhibitors useful in inhibiting AAK1, in.

Supplemental Figures:

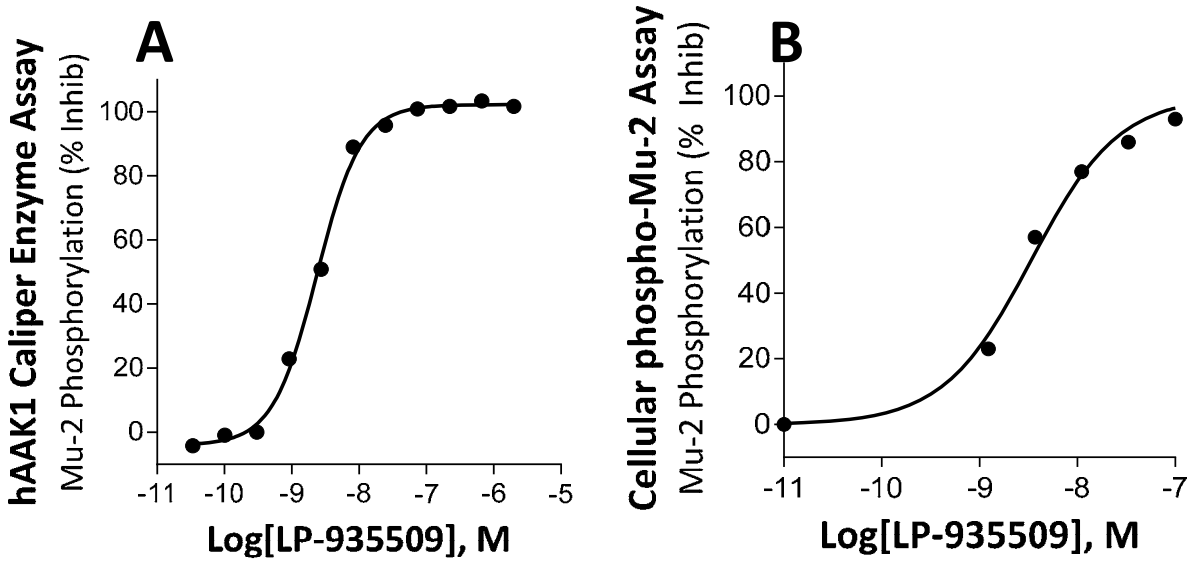

Supplemental Fig. 1. LP-935509 is a potent inhibitor of AAK1 in enzyme and cellular assays

(A) Representative concentration-response curve for inhibition of recombinant AAK1 phosphorylation of μ2 peptide by LP-935509. This assay was repeated eight times with each replicate composed of 11 singlet data points. The LP-935509 IC_{50} was 3.3±0.7 nM (mean ± SEM).

(B) Representative concentration-response curve for inhibition of AAK1 phosphorylation of μ2 protein by LP-935509 in transfected HEK293 cells. This assay was repeated 26 times with each replicate composed of 6 singlet data points. The LP-935509 IC_{50} was 2.8±0.4 nM (mean ± SEM)

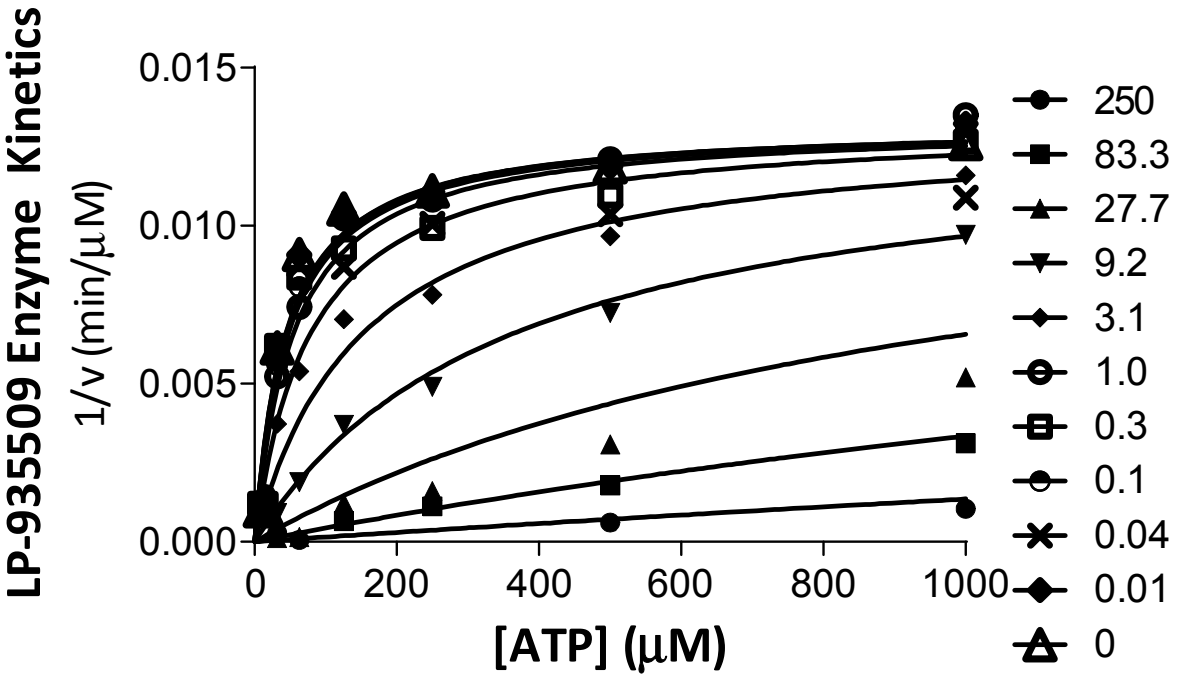

Supplemental Fig. 2. LP-935509 is an ATP competitive inhibitor of AAK1

The *in vitro* activity of AAK1 was measured at various concentrations of ATP and LP-935509 and the results were fit globally to a competitive model of inhibition. The analysis yielded a Ki of 1.3 nM (in good agreement with mean CRC data). The effect of increasing LP-935509 increases the apparent ATP Km while keeping the Vmax largely unchanged, consistent with an ATP competitive mode of inhibition.

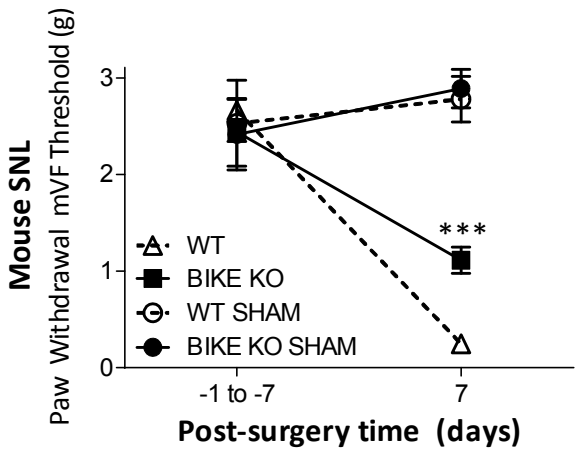

Supplemental Fig. 3. BIKE knockout mice have a modest antinociceptive phenotype in the mouse SNL model

Mechanical allodynia after SNL surgery for wild-type (n=8-11) and BIKE knock out mice (n=12-16). BIKE knockout mice develop only 70% of the mechanical allodynia response in observed wt controls.

***p<0.001 using 2-way RMANOVA with Bonferroni post-hoc WT vs. BIKE KO mice.

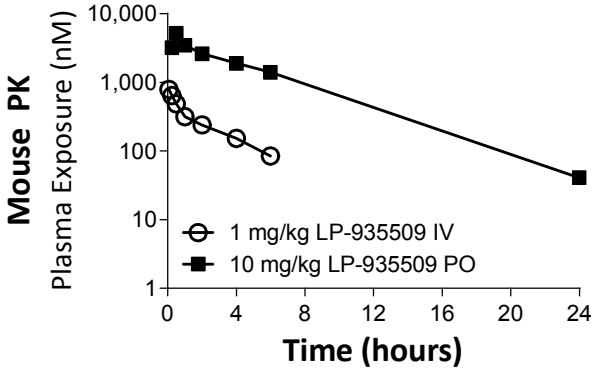

Supplemental Fig. 4. Pharmacokinetics of LP-935509 in mice

Four mice were dosed with LP-935509 either intravenously (1 mg/kg) or orally (10 mg/kg). Blood samples were taken over a 24 hour period and LP-935509 plasma levels were determined. Data were fit to standard PK models. LP-935509 had ~100% oral bioavailability and had a plasma $t_{1/2}$ of 3.6 hr. The Cmax for the 10 mg/kg oral dose was 5.2 μM at 0.5 hours post dose.

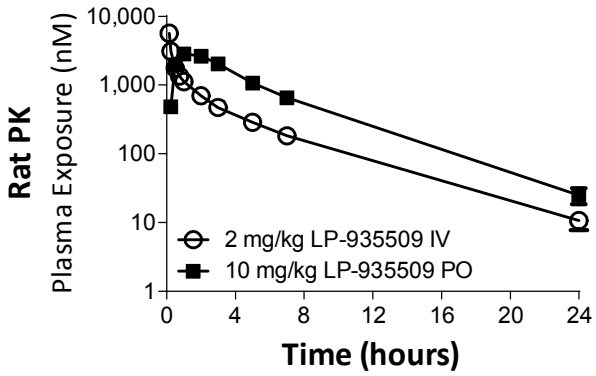

Supplemental Fig. 5. Pharmacokinetics of LP-935509 in rats

Three rats were dosed either intravenously (2 mg/kg) or orally (10 mg/kg). Blood samples were taken at 10 timepoints over a 24 hour period and LP-935509 plasma levels were determined. Data were fit to standard PK models. LP-935509 had 50% oral bioavailability and a plasma $t_{1/2}$ of 4 hr. The Cmax for the 10 mg/kg oral dose was 3.1 uM at 1.3 hours post dose.

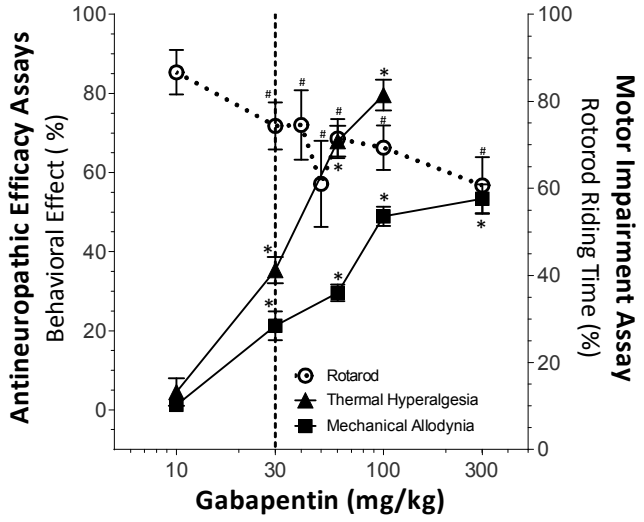

Supplemental Fig. 6. Gabapentin dose-response shows little separation between antineuropathic efficacy and motor impairment on rotarod

A dose-response study of the antineuropathic efficacy of gabapentin (10-300 mg/kg, po) was conducted in rats with nerve injury induced by CCI surgery. Groups of CCI animals were tested separately in assays of thermal hyperalgesia (filled triangles) or mechanical allodynia (filled squares) and both showed dose-dependent relief of pain behavior beginning at 30 mg/kg. A dose-response for motor coordination on the rotarod assay was conducted over these same doses in a parallel cohort of naïve rats (open circles). Naïve animals showed a progressive, dose-dependent deficit in motor function beginning at 30 mg/kg. The minimum efficacious dose for the beneficial antineuropathic activity was also the dose which first showed significant motor impairment (see vertical dashed line). Data were analyzed by 1-way ANOVA followed by Dunnett's test. *$p<0.001$ vs. CCI vehicle (efficacy-vehicle is 0% on Y1-axis) $^{\#}p<0.001$ vs. Naïve vehicle (naïve-vehicle is 100% on Y2-axis).

Supplemental Tables

Supplemental Table 1. Ambit results for LP-935509

Results represent percentage of each kinase bound to beads in the presence of 1 μM LP-935509 compared to control binding reactions lacking compound. Kinases whose binding was significantly inhibited by LP-935509 are highlighted.

Kinase	% Control	Kinase	% Control	Kinase	% Control	Kinase	% Control
AAK1	2.1	EIF2AK1	100	MAP3K5	73	PKN2	82
ABL1		EPHA1	84	MAP3K6	100	PKR	79
ABL1_NPH	67	EPHA2	79	MAPKAPK2	100	PLK1	100
ABL1_PH	100	EPHA3	83	MAPKAPK5	100	PLK2	96
ACK	94	EPHA4	100	MARK1	100	PLK3	100
ACTR2	87	EPHA5	100	MARK2	80	PLK4	71
ACTR2B	69	EPHA6	100	MARK3	96	PRKX	100
ADCK3	81	EPHA7	100	MARK4	100	PRP4	28
ADCK4	81	EPHA8	100	MAST1	82	PYK2	100
AKT1	100	EPHB1	100	MELK	97	QIK	50
AKT2	98	EPHB2	77	MER	100	QSK	100
AKT3	100	EPHB3	100	MET	88	RAF1	60
ALK	100	EPHB4	100	MLK1	100	RET	100
ALK1	100	EPHB6	38	MLK2	96	RHOK	100
ALK2	72	ERK1	100	MLK3	76	RIOK1	3.9

ALK4	93	ERK2	100	MNK1	100	RIOK2	92
AMPKA1	56	ERK3	100	MNK2	100	RIOK3	6.6
AMPKA2	93	ERK4	100	MRCKA	72	RIPK1	99
ANKRD3	70	ERK5	100	MRCKB	90	RIPK2	51
ARG	100	ERK7	78	MSK1_C	67	RIPK5	99
AURA	70	FAK	97	MSK1_N	100	ROCK1	95
AURB	58	FER	100	MSK2_C	100	ROCK2	86
AURC	56	FES	100	MSK2_N	100	RON	100
AXL	100	FGFR1	88	MSSK1	88	ROS	100
BIKE	3.5	FGFR2	82	MST1	40	RSK1_C	100
BLK	100	FGFR3	86	MST2	62	RSK1_N	100
BMPR1A	93	FGFR4	60	MST3	84	RSK2_N	83
BMPR1B	100	FGR	100	MST4	92	RSK3_C	83
BMPR2	72	FLT1	100	MTOR	100	RSK3_N	95
BMX	91	FLT3	100	MUSK	100	RSK4_C	100
BRAF	100	FLT4	99	MYO3A	95	RSK4_N	96
BRK	61	FMS	100	MYO3B	100	SBK	84
BRSK1	93	FRK	63	MYT1	100	SGK085	7.6
BRSK2	82	FUSED	91	NDR1	84	SGK1	100
BTK	68	FYN	49	NDR2	100	SGK110	100
BUB1	74	GAK	42	NEK1	100	SGK2	
CAMK1A	100	GCK	65	NEK10	66	SGK288	13
CAMK1D	100	GPRK4	70	NEK11		SGK3	100
CAMK1G	82	GPRK7	100	NEK2	86	SIK	100
CAMK2A	70	GSG2	80	NEK3	84	SKMLCK	89

CAMK2B	81	GSK3A	100	NEK4	87	SLK	100
CAMK2D	83	GSK3B	62	NEK5	88	SMMLCK	85
CAMK2G	83	HCK	60	NEK6	68	SNRK	100
CAMK4	100	HER2/ERBB2	92	NEK7	100	SRC	100
CAMKK1	77	HER3/ERBB3	100	NEK9	100	SRM	78
CAMKK2	88	HER4/ERBB4	100	NIK	100	SRPK1	19
CAMLCK	100	HH498	60	NIM1		SRPK2	28
CASK	93	HIPK1	92	NLK	100	STK16	55
CDC2L1_ISO4	89	HIPK2	88	NUAK1	65	STK32A	94
CDC2L2_ISO1	100	HIPK3	47	NUAK2	100	STK33	100
CDC2L5	95	HIPK4	99	OSR1	100	STLK3	88
CDK11	60	HPK1	80	P38A	94	SYK	100
CDK2	99	HUNK	56	P38B	89	TAK1	100
CDK3	92	ICK	100	P38D	100	TAO1	60
CDK4-CCND1	64	IGF1R	100	P38G	100	TAO2	64
CDK4-CCND3	100	IKKA	67	P70S6K	100	TAO3	75
CDK5	100	IKKB	61	PAK1	100	TBK1	78
CDK7	100	IKKE	69	PAK2	100	TEC	90
CDK8	55	INSR	95	PAK3	100	TESK1	93

CDK9	93	IRAK1	80	PAK4	62	TGFBR1	64
CDKL1	100	IRAK3	88	PAK5	100	TGFBR2	100
CDKL2	53	IRAK4	100	PAK6	97	TIE1	100
CDKL3	84	IRE1	67	PCTAIRE 1	100	TIE2	98
CDKL5	94	IRR	96	PCTAIRE 2	100	TLK1	97
CHK1	100	ITK	100	PCTAIRE 3	100	TLK2	72
CHK2	77	JAK1	100	PDGFRA	100	TNK1	100
CK1A	100	JAK1_PSEU DO	48	PDGFRB	83	TRKA	61
CK1A2	100	JAK2	89	PDK1	82	TRKB	40
CK1D	85	JAK3_D2	71	PFTAIRE 1	90	TRKC	50
CK1E	86	JNK1	100	PFTAIRE 2	100	TRPM6	100
CK1G1	77	JNK2	100	PHKG1	100	TSSK1	54
CK1G2	100	JNK3	100	PHKG2	100	TTK	100
CK1G3	92	KDR	100	PI3KC2B	92	TXK	74
CK2A1	79	KHS1	76	PI3KC2G	94	TYK2	76
CK2A2	62	KHS2	74	PI3KCA	81	TYK2_PSEU DO	74
CLIK1	68	KIT	84	PI3KCB	100	TYRO3	100
CLK1	81	LATS1	100	PI3KCD	68	ULK1	94
CLK2	100	LATS2	82	PI3KCG	100	ULK2	70

CLK3	78	LCK	100	PI4KCB	100	ULK3	54
CLK4	98	LIMK1	100	PIM1	100	VRK2	99
CRIK	92	LIMK2	94	PIM2	100	WEE1	82
CSK	100	LKB1	9.7	PIM3	100	WEE1B	100
CTK	46	LOK	63	PIP5K1A	100	WNK1	74
DAPK1	82	LRRK2	87	PIP5K1C	53	WNK3	53
DAPK2	86	LTK	68	PIP5K2B	71	YANK2	98
DAPK3	98	LYN	79	PIP5K2C	9.5	YANK3	62
DCAMKL1	99	LZK	98	PKACA	66	YES	100
DCAMKL2	100	MAK	100	PKACB	100	YSK1	65
DCAMKL3	100	MAP2K1	100	PKCD	83	YSK4	100
DDR1	100	MAP2K2	91	PKCE	76	ZAK	78
DDR2	36	MAP2K3	80	PKCH	49	ZAP70	88
DLK	100	MAP2K4	100	PKCI	90	ZC1/HGK	83
DMPK1	98	MAP2K5	65	PKCT	100	ZC2/TNIK	83
DMPK2	97	MAP2K6	56	PKD1	100	ZC3/MINK	96
DRAK1	6.4	MAP2K7	92	PKD2	100		
DRAK2	30	MAP3K1	49	PKD3	100		
DYRK1A	95	MAP3K15	86	PKG1	100		
DYRK1B	65	MAP3K2	100	PKG2	88		
DYRK2	63	MAP3K3	100	PKN1	90		
EGFR	89	MAP3K4	73	PKN2	100		

Supplemental Table 2. Liability screen results for LP-935509

Assay	**LP -935509 IC_{50}, μM**
Adenosine A2a	28
Adrenergic Alpha 1B	>30
Adrenergic Alpha 1D	>30
Adrenergic Alpha 2A	>30
Adrenergic Alpha 2C	>30
Adrenergic beta 1	>30
Adrenergic beta 2	>30
Cannabinoid CB1	>30
Dopamine D1	>30
Dopamine D2	>30
Histamine H1	>30
Histamine H2	>30
Muscarinic M2	23
Opiate Kappa	30
Opiate Mu	>30
Serotonin 5HT1B	>30
Serotonin 5HT2A	>10
Serotonin 5HT2B	>10
Serotonin 5HT4	>30
DAT	29
NET	22

5HTT SERT	>30
Androgen Receptor	>150
Estrogen ERalpha	>150
Glucocorticoid Receptor	>150
Progesterone Receptor	94
L-type Ca2+ Channel	12
GABA-A (a1b2g2) Antagonist	>30
GABA-A (a1b2g2) Potentiator	12.1
GABA-A (a2b2g2) Potentiator	12.2
GABA-A Alpha 5channel	>30
NMDA 1.2A Channel	>25
NMDA 1.2B Channel	>25
Cardiac Na+ Channel	>30
Nicotinic Ach alpha1 channel	12
Nicotinic Ach alpha7 channel	24
Nicotinic Acetylcholine a4b2	>30
T-Type Calcium	>25
Acetylcholinesterase	>60
MAO-A	>30
MAO-B	>30
PDE3	11
PDE4	8.3

Supplemental Table 3. Drug levels for in vivo experiments

Mouse Formalin (Fig. 3A). LP935509, 4 samples/dose					
Dose (mg/kg)	Time post dose (min)	Ave (SD) Plasma Drug level (nM)	Ave (SD) Brain Drug level (nM)	Ave Free Plasma Drug level (nM)	Free Plasma Drug level/Cellular IC_{50}
10	60	4,100 (1200)	16,000 (6900)	90	32
30	60	13,000 (2300)	61,000 (9700)	280	101
60	60	23,000 (5800)	115,000 (21,000)	510	190
Mouse SNL (Fig. 3B). LP935509, 4 samples/time					
10	30	3,600	14,000	79	29
30	30	8,200	35,000	180	65
60	30	15,000	62,000	340	120
10	120	3,300	11,000	72	26
30	120	6,300	28,000	140	50
60	120	13,000	52,000	280	100
Mouse Open Field (Fig. 3C). LP935509, 3 samples/time					
10	60	3,500 (980)	14,000 (2800)	76	28
30	60	12,000 (1400)	48,000 (16,000)	264	95

60	60	15,000 (2300)	60,000 (11,000)	338	122
Rat Thermal Hyperalgesia (Fig. 6A). LP935509, 7 samples/time					
0.1	180	9	BLQ	0.2	0.1
0.3	180	37	170	1	0.4
1	180	44	310	1.1	0.4
3	180	290	1,010	7.6	2.8
10	180	810	3,300	21	7.6
30	180	2,400	8,500	62	22
Rat CCI Cold Allodynia (manual) (Fig. 6B). LP935509, 5 samples/time					
1	240	100 (20)	430 (50)	2.6	0.9
3	240	300 (200)	1000 (680)	7.8	2.8
10	240	1090 (660)	3,700 (2,500)	28	10
30	240	3,500 (1200)	10,000 (3,600)	92	33
Rat CCI Mechanical Allodynia (manual) (Fig. 6C). LP935509, 5 samples/time					
1	240	170 (40)	470 (80)	4.4	1.6
3	240	560 (110)	1,100 (160)	14.6	5.3
10	240	2100 (650)	3,800 (880)	55	20
30	240	4800 (1900)	7,600 (3,700)	125	45

Rat CCI Mechanical Hyperalgesia (Fig. 6D). LP935509, 4 samples/time					
3	210	400 (100)	1400 (200)	10	3.8
10	210	1,400 (200)	4,500 (800)	36	13
30	210	3,700 (7000	7,300 (4600)	96	35
Rat Rotarod (Fig. 6E). LP935509, 5-7 samples/time					
10	180	860 (360)	3,600 (1600)	22	8
30	180	3200 (840)	12,000 (230)	84	30
60	180	2900 (1300)	10,300 (4400)	75	27
Rat STZ (Fig. 6F). LP935509, 4 samples/time					
1	240	90 (40)	420 (270)	2.3	0.8
3	240	320 (160)	950 (400)	8.3	3
10	240	3,100 (1,100)	5040 (100)	81	29
30	240	16,000 (6070)	29,000 (7,500)	423	153
Mouse SNL (Fig. 7A) LP-927761 3 samples/time					
60	120	11,000 (4,500)	77 (23)	1246	164

Supplemental Table 4. Drug levels for animals used in study in Fig. 7B

6 animal/condition, 30 min post dose						
Compound	Dose (μg)	Ave (SD) Plasma Drug level (nM)	Ave (SD) Brain Drug level (nM)	Ave (SD) CSF Drug level (nM)	Ave (SD) Lumbar Spinal Cord Drug level (nM)	Ave (SD) Thoracic Spinal Cord Drug level (nM)
BMS-090605	0.3	3.3	BLQ[2]	BLQ[2]	90.8 (85.6)	BLQ[2]
BMS-090605	1	3.7 (1.3)	BLQ[2]	BLQ[2]	317 (444)	BLQ [2]in 4 rats
BMS-090605	3	3.2 (1.1)	BLQ[2]	BLQ[2]	229 (336)	BLQ[2]
Clonidine	3	BLQ[1]	BLQ[3]	BLQ[3]	3209 (1870)	BLQ[3]

1. BLQ <19.53 nM
2. BLQ <6.21 nM
3. BLQ <97.65 nM

Supplemental Table 5. Drug levels for animals used in study in Fig. 9B

4 animals per group, 1.5 h post experiment					
Group	Analyte	Dose (mg/kg)	Ave (SD) Plasma Drug level (nM)	Ave (SD) Brain Drug level (nM)	Ave (SD) Thoracic Spinal Cord Drug level (nM)
Yohimbine	Yohimbine	1	1100 (280)	480 (140)	450 (60)
LP-935509 pretreated with yohimbine	Yohimbine	1	1100 (110)	470 (70)	510 (35)
	LP-935509	30	1800 (180)	4700 (770)	5600 (350)
Yohimbine + Tizanidine*	Yohimbine	1	990 (290)	300 (210)	300 (20)
LP-935509 + Saline	LP-935509	30	2100 (550)	5300 (1300)	6400 (1700)

Supplemental Table 6. Drug levels for satellite animals for Fig. 5(A)

Dose (mg/kg)	Time since last dose (min)	Dosing Day	Ave Plasma Drug level (nM) (n=2 per group)	Ave Brain Drug level (nM) (n=2 per group)
3	30	1	740	2,400
10	30		3200	9,050
30	30		5700	21,000
3	120		510	1,900
10	120		2200	7,500
30	120		6000	24,000
3	180		520	2,300
10	180		1600	6,100
30	180		4200	15,000
3	30	2	3500	3,900
10	30		3600	8,900
30	30		8000	30,600
3	120		2000	2,800
10	120		2400	7,000
30	120		5800	18,000
3	30	3	1100	3,800
10	30		3400	9,900
30	30		9400	37,000
3	120		520	2,100

10	120		1700	4,800
30	120		7400	24,000
3	30	4	760	2,200
10	30		2300	6,200
30	30		5600	15,000
3	120		610	1,900
10	120		1900	5,600
30	120		5300	19,000
3	30	5	910	2,900
10	30		3000	8,700
30	30		7700	38,000
3	120		370	1,300
10	120		1800	5,800
30	120		5900	19,000